Geomorphology 264 (2016) 80–94

Contents lists available at ScienceDirect

Geomorphology

journal homepage: www.elsevier.com/locate/geomorph

Synergic use of satellite and ground based remote sensing methods for monitoring the San Leo rock cliff (Northern Italy)

William Frodella *, Andrea Ciampalini, Giovanni Gigli, Luca Lombardi, Federico Raspini, Massimiliano Nocentini, Cosimo Scardigli, Nicola Casagli

Department of Earth Sciences, University of Florence, Via G. La Pira 4, 50121 Florence, Italy

ARTICLE INFO

Article history:
Received 1 September 2015
Received in revised form 7 April 2016
Accepted 8 April 2016
Available online 14 April 2016

Keywords:
Rock fall
Radar interferometry
Laser scanning
Marecchia River valley

ABSTRACT

The historic town of San Leo (Emilia Romagna Region, northern Italy) is located on top of an isolated rock massif above the Marecchia River valley hillside. On February 27th 2014, a northeastern sector of the massif collapsed; minor structural damages were reported in the town and a few buildings were evacuated as a precautionary measure. Although no fatalities occurred and the San Leo cultural heritage suffered no damage, minor rock fall events kept taking place on the newly formed rock wall, worsening this hazardous situation. In this framework, a monitoring system based on remote sensing techniques, such as radar interferometry (both spaceborne and ground-based) and terrestrial laser scanning, was planned in order to monitor the ground deformation of the investigated area and to evaluate the residual risk. In this paper the main outlines of a 1-year monitoring activity are described, including a pre-event analysis of possible landslide precursors and a post-event analysis of the displacements of both the collapse-affected rock wall sector and the rock fall deposits.

1. Introduction

The overlapping of hard-brittle rock masses on soft plastic bedrock represents one of the most critical environments for slope instability, due to the different response of the materials to disturbances such as weathering, erosion, seismic shocks or man-made excavations. This geological setting tends to form a peculiar landscape characterized by rock hilltops (plateaus or buttes), bounded by steep rock cliffs located above the surrounding erodible hillside. The sub-vertical and jointed rock walls can be affected by a variety of mechanisms such as rock falls, rock slides, toppling (either forward or back tilting) and differential settlements (Cancelli and Pellegrini, 1987; Cruden and Varnes, 1996; Gigli et al., 2012; Hungr et al., 2001, 2014). The whole hilltop may be affected by lateral spreading, whereas the soft bedrock may undergo squeezing out and bulging (Pasek, 1974; Zaruba and Mencl, 1982; Pasuto and Soldati, 1996, 2013). This situation provides potential material which can be involved in the failure mechanisms taking place in the underlying clayey bedrock, such as rotational or compound slides and earth flows (Hutchinson, 1988; Cruden and Varnes, 1996; Hungr et al., 2001, 2014). The latter instability mechanisms may also be influenced by the accumulation of material fallen from the rock cliff, causing surcharge (Zaruba and Mencl, 1982). In this framework the worst-risk scenario may be represented by the collapse of large rock mass portions of the plateau borders. Such a configuration generates high hazard conditions associated with a marked vulnerability and related risk for the structures built on the hilltops, particularly regarding cultural heritage; not to mention threats to people's safety. In Europe several historical castles or ruins are located on steep cliffs affected by instability processes (Vlcko, 2004; Vlcko et al., 2008; Egglezos et al., 2008; Panzera et al., 2012). In particular cultural heritage in Italy including castles, churches and entire historical cities is often found on hilltops suffering instability, requiring expensive maintenance and restoration works (Cestelli-Guidi et al., 1984; Cotecchia, 1997; Paolucci, 2002; Tommasi et al., 2006; Ciampalini et al., 2012; Bianchini et al., 2014).

The protection and preservation of cultural heritage from natural hazards requires a specific monitoring system, which should be designed considering: i) the site's characteristics (topography and geological setting); ii) instability phenomena features (kinematics, magnitude and velocity); iii) typology of the related hazard affecting each specific area of interest. Advanced remote sensing techniques such as multi-interferometric satellite Synthetic Aperture Radar (such as PS-InSAR), ground-based interferometric SAR (GB-InSAR) and terrestrial laser scanning (TLS) can play an important role in landslide risk management, as they allow for the representation of large surfaces with dense spatial sampling, offering clear advantages with respect to traditional topographical systems such as GPS and total stations. These latter on the contrary provide accurate data but are necessarily limited to a small number of control points (Teza et al., 2008; Piacentini et al., 2015).

The PS-InSAR technique is commonly used to monitor the safety of the cultural heritage affected by instability phenomena for its capability to detect, analyse and quantify displacements during pre- and post-

* Corresponding author.
E-mail address: william.frodella@unifi.it (W. Frodella).

http://dx.doi.org/10.1016/j.geomorph.2016.04.008

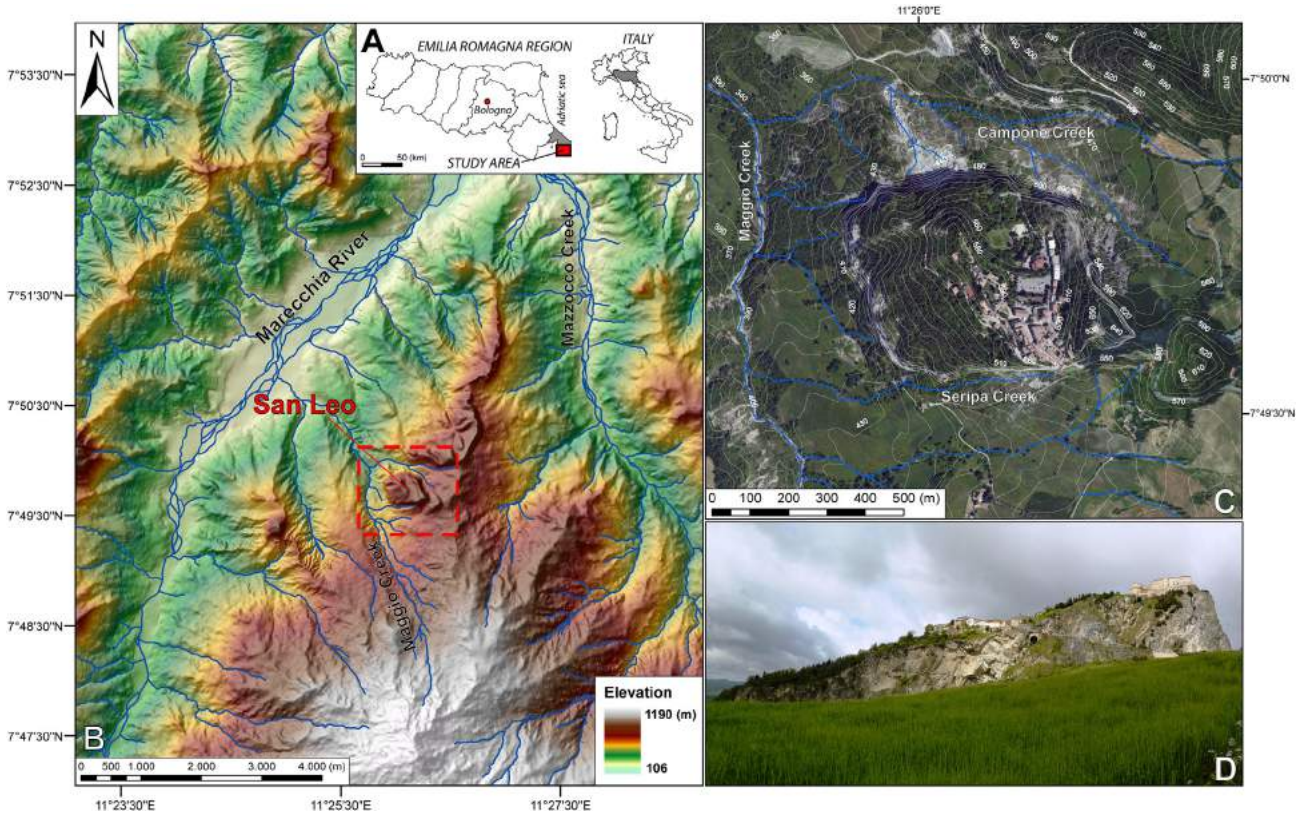

Fig. 1. Study area. (A) Geographical location in Italy. (B) Geomorphological setting. (C) Contour map projected on an orthophoto. (D). South side of the San Leo rock massif with the fortress on the right.

event phases through long time deformation series (covering more than 20 years) over large areas (Del Ventisette et al., 2013). For example PS-InSAR technique was used to monitor the slope instability of the archeological area of Petra, Jordan (Delmonaco et al., 2015), to analyse the San Fratello town's historical building deformation (Bianchini et al., 2014) in Southern Italy, and the stability of historical towns located on hilltops such as Volterra, Central Italy (Bianchini et al., 2015), and Citadel and Mdina fortifications in the island of Malta (Gigli et al., 2012). For its capability to measure displacements with high geometric accuracy and temporal sampling frequency, and for its adaptability to specific applications, GB-InSAR represents a powerful terrestrial technique successfully employed in engineering and geological analysis to detect fast structural deformation (Broussolle et al., 2014) and ground displacements (Tarchi et al., 1997, 2000, 2002; Pieraccini et al., 2000, 2002). This technique has proven its effectiveness for landslide and volcanic flank monitoring (Intrieri et al., 2012; Nolesini et al., 2013; Di Traglia et al., 2014), as well as for analyzing the stability of isolated hilltops on which historical towns are built (Luzi et al., 2004; Fanti et al., 2013; Pratesi et al., 2015). The TLS technique is increasingly being used for instability analyses in cultural heritage sites (Boehler et al., 2001; Arayici, 2007; Lambers et al., 2007; Yastikli, 2007; Al-kheder et al., 2009; Gigli et al., 2012; Fanti et al., 2013; Gigli et al., 2014; Pratesi et al., 2015), as it allows for a highly accurate 3D representation of both the underlying ground and the overlying structures in a short time.

The town of San Leo, renowned for its medieval fortress and Romanesque churches, is located in the south-eastern sector of the Emilia Romagna region (Northern Italy). Due to its peculiar geological and geomorphological setting, San Leo represents an interesting case for the issue of cultural heritage conservation in the face of slope instability. The town lies on an isolated rock massif historically affected by instability phenomena: rock falls, slides and topples have taken place along the hilltop boundaries, with the consequent retreat of the bordering cliffs and their continuous reshaping with the formation of ledges, overhangs and niches (Nesci et al., 2005). This ongoing process threatens the buildings and the structures near the cliff, and occasions the expensive maintenance and consolidation works necessary to avoid damage to the old town and fortress (Ribacchi and Tommasi, 1988; Caturani et al., 1991; Benedetti et al., 2013).

On February 27th 2014, an entire north-eastern sector of the rock plate collapsed causing a huge rock fall of about 0.33 Mm^3 (Borgatti et al., 2015). This rock fall event caused a retreat of the cliff edge, threatening some buildings. Therefore a ground displacement monitoring activity was initiated, in order to manage the post-event emergency phase and evaluate the residual risk. The monitoring activities consisted of i) a pre-event displacement characterization by acquiring archival spaceborne SAR images; and ii) a post-event displacement analysis by means of a real time GB-InSAR monitoring coupled with TLS surveys.

2. Study area

The town of San Leo is located on the right side of the mid Marecchia River valley, between the Emilia-Romagna and Marche regions, about 135 km southeast of Bologna and 30 km southwest of the Adriatic coastline (Fig. 1A,B). The site lies on a hilltop constituted by a rock plate of quadrangular shape, about 0.3 km^2 in extension, bordered by subvertical and overhanging cliffs up to 100 m high (Fig. 1C,D). The rock plate is delimited on the west, north and south sides respectively by creek valleys of small tributaries entering the Marecchia River from its right bank (Fig. 1C), and it rises from the surrounding hillside to the height of about 650 m a.s.l. Given its strategic location, the site has hosted urban settlements since the Roman times; its medieval fortress and Romanesque abbey church in particular, make San Leo one of the most important touristic sites in central Italy (Benedetti et al., 2013; Borgatti et al., 2015).

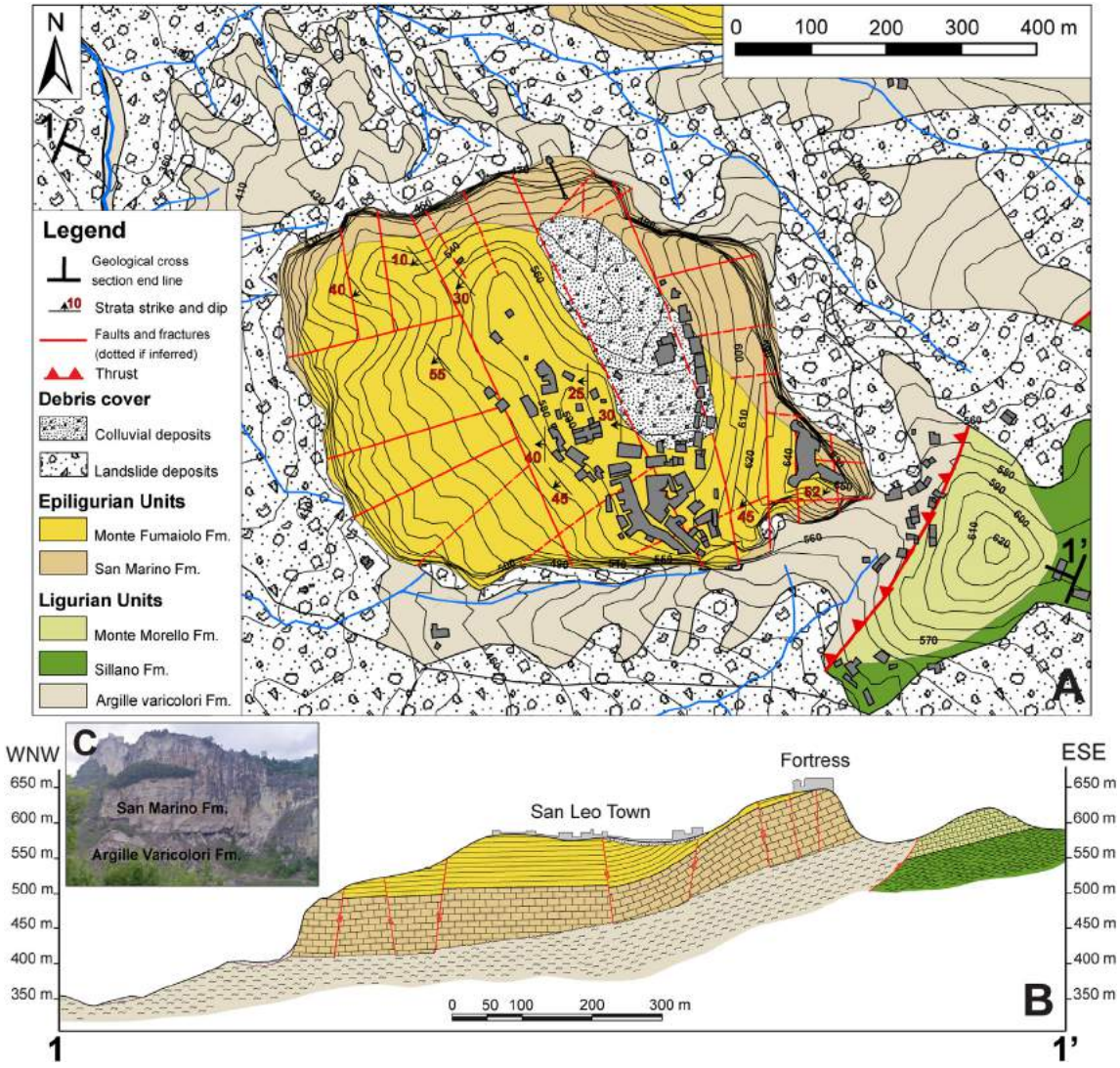

Fig. 2. Geology of the study area. (A) Geological map. (B) Cross section (modified after Conti and Tosatti, 1996). (C) Picture of the NE rock plate sector bordering the slope wall prior to the landslide event.

2.1. Geological setting

From a geologic point of view the San Leo rock plate is made of limestone-arenaceous formations (Epiligurian Units), overlying soft ductile clayey deposits (Ligurian Units), which amply crop out in the gentle hills and surrounding badlands (Fig. 2A,B). The Epiligurian Units are represented, from top to bottom, by the Mt. Fumaiolo Formation (glauconitic sandstone with thin siltstone interlayers and calcarenite), which mainly constitute the top of the massif, and the San Marino Formation (thick-bedded organogenic calcirudite and calcarenite), mainly forming the bordering rock walls (Conti, 1989, 2002; De Feyter, 1991; Conti and Tosatti, 1996; Cornamusini et al., 2010). The latter formation lies uncomformably on top of the Ligurian Units bedrock, mainly composed by the Argille Varicolori Formation (highly tectonized clay, with marly and limy sandstone), whereas in the SE sector of the site the Sillano Formation (mudstone with thin limestone and marly layers) and the Mt. Morello Formation (carbonate turbidites) also crop out (Ponzana, 1993; Cornamusini et al., 2010; De Capoa et al., in press) (Fig. 2A,C). The rock plate structural setting is characterized by NW–SE and WSW–ENE trending faults and fractures dissecting the rock plate, whereas the strata mainly dip SW from low to middle angles (Conti and Tosatti, 1996) (Fig. 2A).

2.2. Geomorphological features and instability phenomena

The geological and structural settings of the study are control features for the geomorphology and slope instability phenomena, as also found in other isolated steep hilltops (buttes or plateaus) particularly in the northern Apennines and the Marecchia River valley (Bertocci et al., 1991; Casagli et al., 1994; Canuti et al., 1990, 1999, 2004; Nesci et al., 2005; Giardino et al., 2015).The different resistance to weathering and erosional processes of the outcropping lithotypes enhances selective erosion in the soft clayey bedrock, shaping the hillsides by mass movements, causing widespread badlands growth, and undermining the overlying brittle rock plate (Nesci et al., 2005; Benedetti et al., 2013; Spreafico et al., 2013). The latter process causes the opening and widening of sub-vertical joints and fractures in the brittle rock mass, producing stress redistribution and lateral spreads which isolate large rock blocks. These can be involved in vertical relative displacements due to local elastic-viscous settlements and yielding (Casagli et al., 1994), and in marginal mass movements corresponding to the boundary between the rock plate and the bedrock (Gigli et al., 2012).

During the last four centuries several large landslides (rock falls, earth flows and complex landslides) have affected the San Leo cliff and the surrounding clayey bedrock (Benedetti et al., 2013; Spreafico et al., 2013; Giardino et al., 2015; Borgatti et al., 2015). Ancient rock

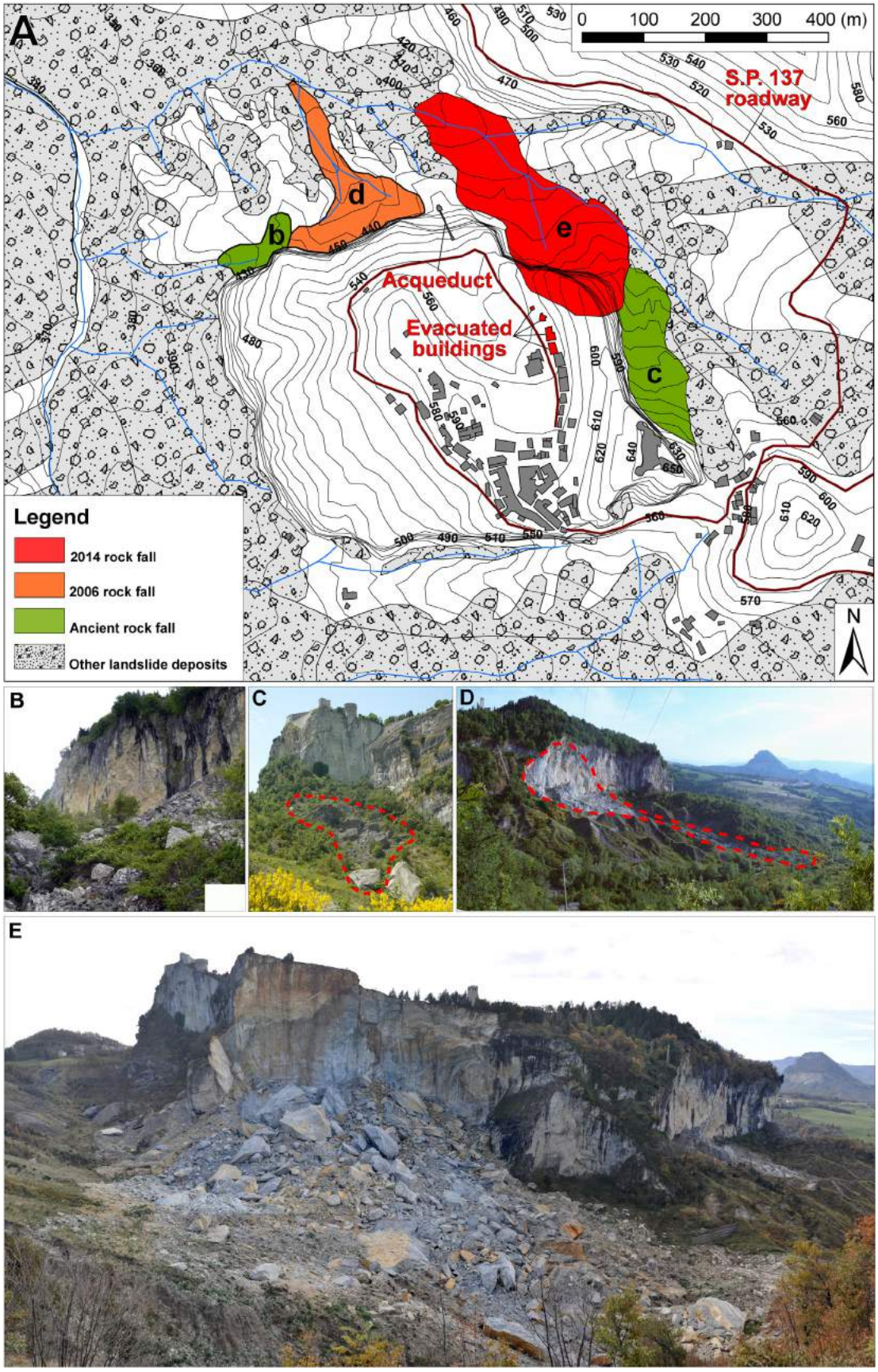

Fig. 3. Instability phenomena affecting the San Leo rock plate boundaries. (A) Map. Modified after the IFFI project to produce an inventory of landslides in Italy, carried out by ISPRA (Istituto Superiore per la Protezione e la Ricerca Ambientale) (Trigila et al., 2010). (B, C) Pictures of ancient rock fall deposits shown as "b" and "c" in A. (D) Rock fall and earth flow caused on May 11th 2006. Dashed red line roughly delimits the accumulated deposits mapped as "d" in A. (E) Rock fall caused on February 27th 2014, mapped as "e" in A.

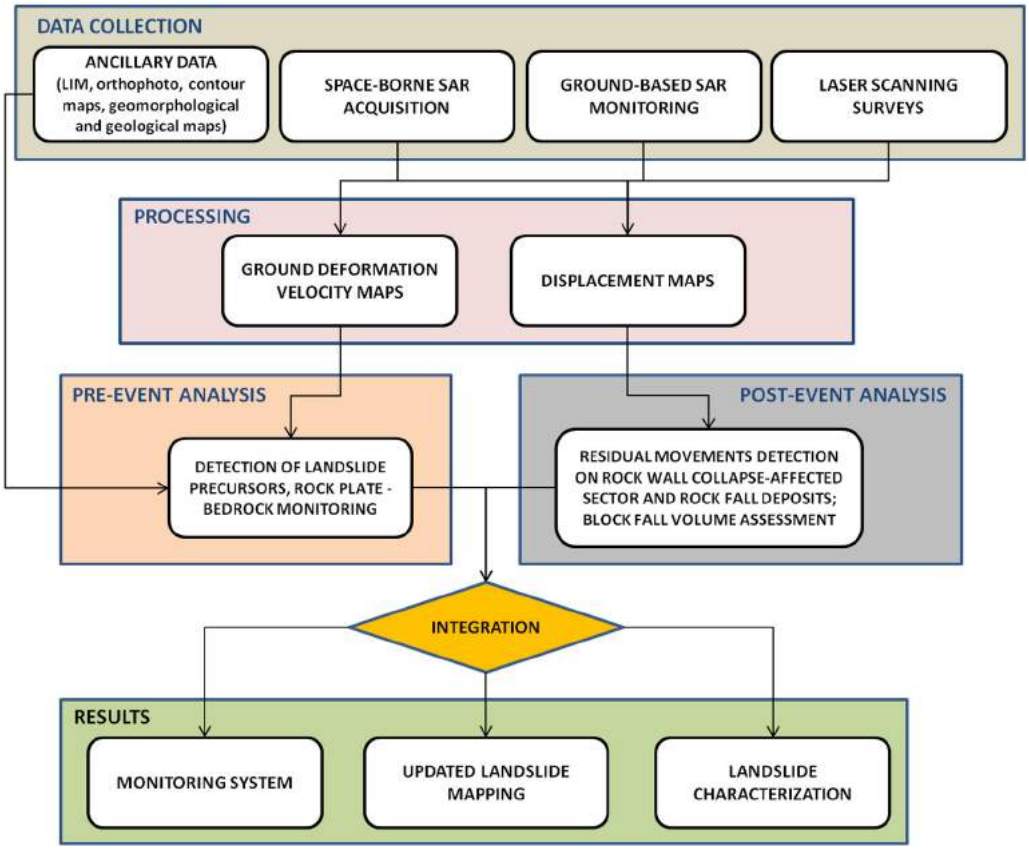

Fig. 4. Work flow of the applied monitoring system.

fall deposits with metric size boulders are still visible at the foot of the cliff on both the north-western rock wall sector and the north-eastern sector below the fortress (Fig. 3A,B,C; Benedetti et al., 2013). More recently, on May 11th 2006, a significant rock fall of about 50,000 m^3 affected the northern cliff sector, triggering a large earth flow in the underlying clayey slopes which evolved downstream in the Campone Creek valley (Figs. 1C and 3A,D) (Benedetti et al., 2013; Borgatti et al., 2015). The rock fall event on February 27th 2014 took place in an uninhabited area of the San Leo rock plate and no fatalities or injuries occurred. The cultural heritage suffered no damage after the event, but minor structural damage was reported to the town aqueduct and power plant electric cables. The rock fall material, formed by huge over ten meter boulders ended in the Campone Creek valley below. As a precautionary measure the access to the fortress and provincial SP 137 roadway (located about 300 m opposite to the landslide affected rock wall; Fig. 3A) was temporarily prohibited, and three buildings located near the newly formed landslide scarp were evacuated (Borgatti et al., 2015).

3. Methodology

3.1. PSInSAR

The advanced multi-interferometric SAR technique known as Permanent Scatterer Interferometry (PS-InSAR) is commonly used in landslide studies for its ability to measure ground displacements with millimeter accuracy (Costantini et al., 2000; Ferretti et al., 2000, 2005; Hanssen, 2005; Raucoules et al., 2007; Crosetto et al., 2010). For example PS-InSAR technique is used in the field of engineering geology to study land subsidence (Herrera et al., 2010; Raspini et al., 2012, 2014), earthquake-related ground deformation (Bűrgmann et al., 2005; Sousa et al., 2010), volcanic activities (Hooper et al., 2004; Vilardo et al., 2010; Parker et al., 2014) and landslides (Meisina et al., 2013; Ciampalini et al., 2014; Bardi et al., 2014). The multi-interferogram approach, such as the PS-InSAR technique relies on the identification of stable radar targets, the so-called Permanent Scatterers (PSs) characterized by a stable phase signal (Ferretti et al., 2001; Hooper et al., 2004; Meisina et al., 2008). The multiple differential interferograms approach allows for a high precision series of ground deformation in an investigated area over a long time. PS-InSAR makes it possible to measure the movements of each PS along the satellite Line Of Sight (LOS) with respect to an assumed stable point (Massironi et al., 2009). PS targets are represented by anthropic (buildings, metallic structures) or natural objects (rock outcrops) which are scatterers with a stable radar signature (Ferretti et al., 2000). This means that urbanized areas include a high number of PS, on the contrary vegetated, rural and forested areas, show a lower amount of PS reducing the applicability of the technique. SAR sensors capture images laterally to the left and/or right following a North-South oriented orbit. Thus, the technique is useful to detect ground deformation located on prevalently east- or west-facing slopes.

Table 1
Characteristics of the satellites used for the Squee-SAR monitoring of San Leo hilltop during the pre-event phase.

Wavelength range (cm)	Revisiting time (days)	Geometry	Incidence angle θ (°)	Time interval	No. of scenes
3.75–2.5	16	Ascending	31	09/05/2011–26/02/2014	39
		Descending	26	13/03/2010–06/01/2014	35

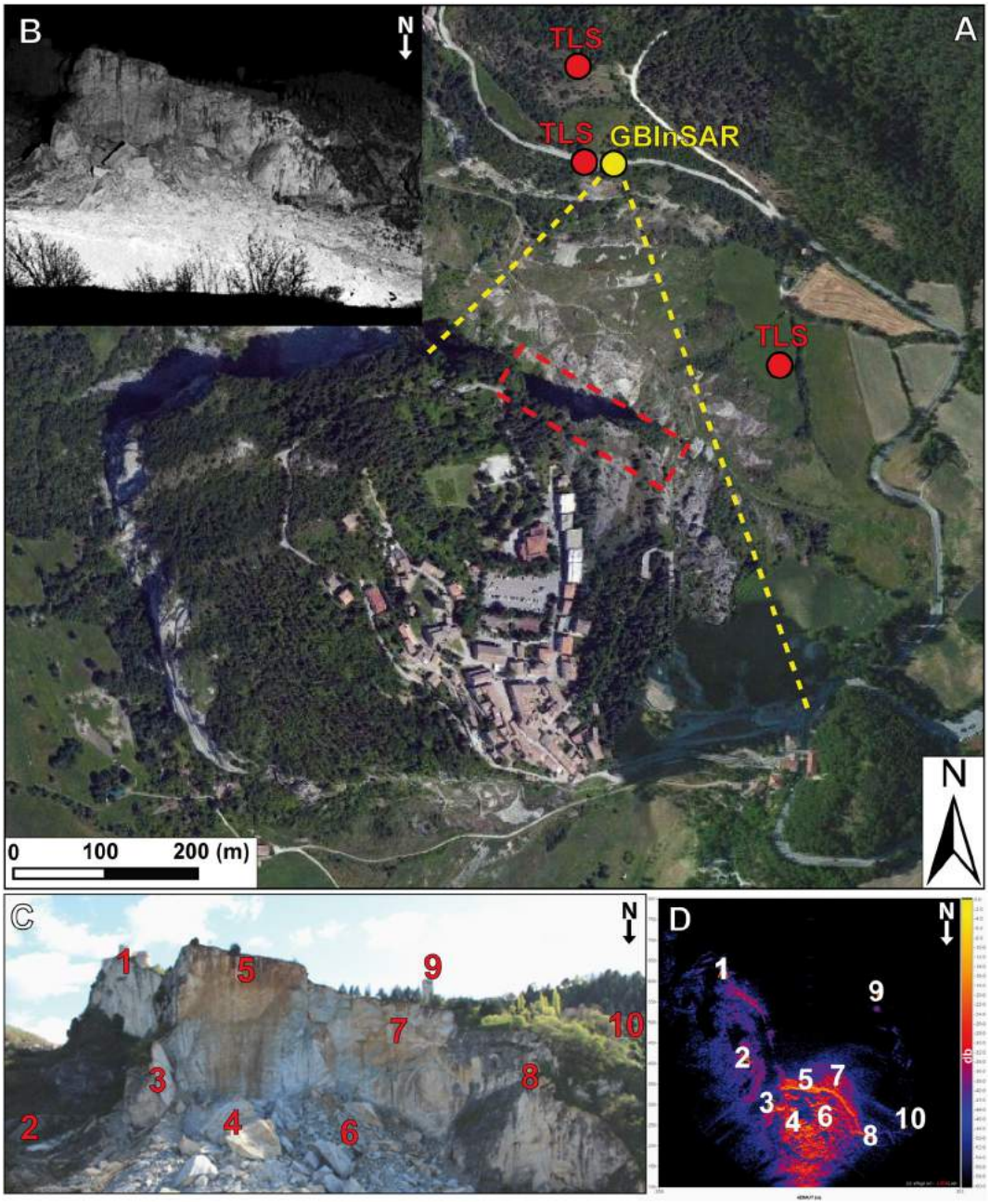

Fig. 5. Description of the monitoring system. (A) Location of the employed terrestrial monitoring devices. The collapsed cliff sector is enhanced with a dashed red square. TLS = Terrestrial Laser Scanning; GB-InSAR = Ground Based Radar. (B) Point cloud, (C) optical image and (D) SAR image of the scanned area. Numbers in C correspond to those in D 1 = fortress. 2 = ancient rock fall deposits. 3, 4, 6 = 2014 rock fall deposits (3 = deca-metric rock block; 4, 6 = scattered metric blocks). 5, 7 = 2014 collapse-affected rock wall sectors. 8, 10 = rock wall and vegetated areas without collapses. 9 = abbey church bell tower.

Another limitation of the PS-InSAR technique is represented by geometric distortions affecting SAR images (namely foreshortening, layover and shadowing effects). These effects are frequent in radar images and occur especially where SAR sensor illuminates mountainous slopes or target areas with different incidence angles. The Squee-SAR algorithm is a new advanced multi-temporal interferometric technique which measures ground displacements using both PSs and the Distributed Scatterers (DSs). The latter correspond to homogeneous areas spread over a group of pixels in a SAR image (rangeland, pasture, shrubs and bare soils). This innovative approach allows increasing the point target density with respect to the traditional PS-InSAR technique, especially in the case of sparse vegetation landscapes (Tofani et al., 2013; Bellotti et al., 2014; Notti et al., 2014).

3.2. GB-InSAR

A GB-InSAR system consists of a computer-controlled microwave transceiver, characterized by a transmitting and receiving antenna, which can synthesize a linear aperture along the azimuth direction by moving along a mechanical linear rail. A SAR (Synthetic Aperture Radar) image is obtained by combining the spatial resolution along the direction perpendicular to the rail (range resolution, ΔRr), and that parallel to the synthetic aperture (azimuth or cross-range resolution, ΔRaz). This image contains amplitude and phase information of the observed object-backscattered echo within the investigated scenario in the acquiring time interval. The working principle of the GB-InSAR technique is the evaluation of the phase difference, pixel by pixel,

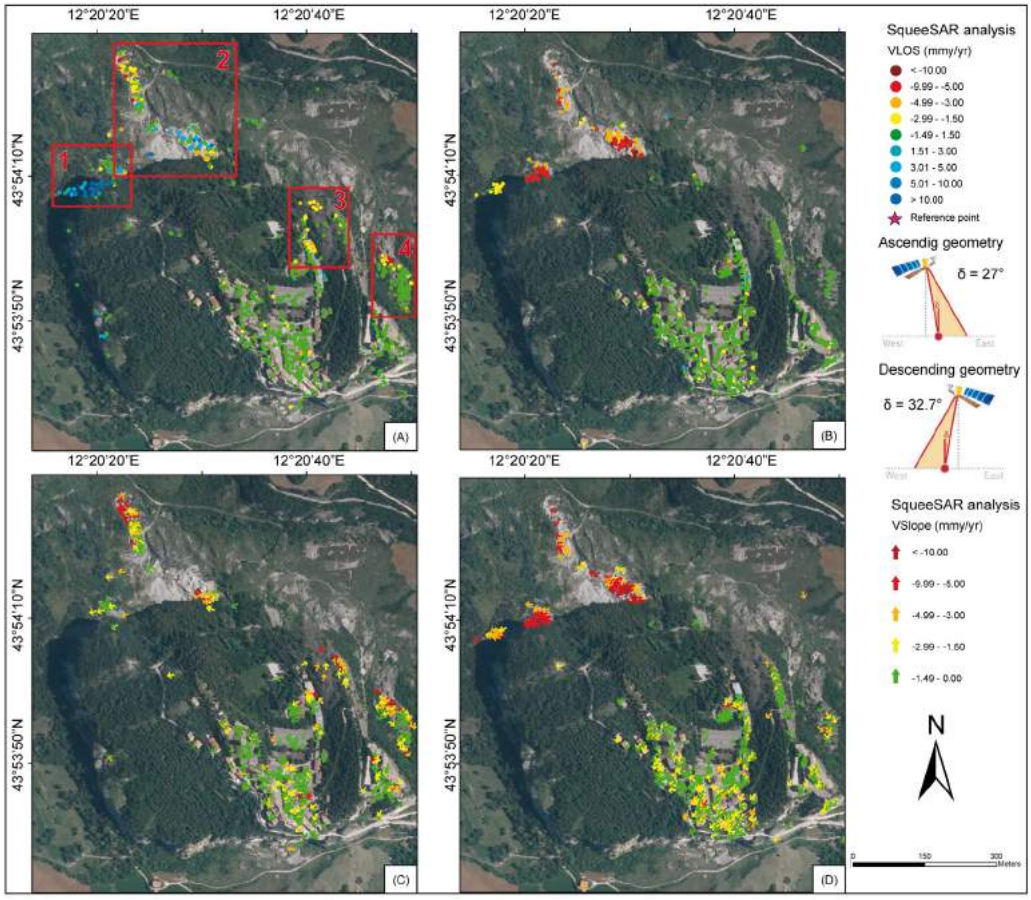

Fig. 6. COSMO-SkyMed velocity maps for the San Leo rock plate. (A) Ascending geometry 1, 4: ancient rock fall deposits; 2: 2006 rock fall-earth flow; 3: rock plate sector affected by the 2014 rock fall). (B) Descending geometry. (C) V_{slope} velocity maps for ascending geometry. (D) V_{slope} velocity maps for descending geometry.

between two pairs of averaged sequential SAR images of the same scenario, which constitutes an interferogram (Bamler and Hartl, 1998). In the time elapsed between the acquisition of two or more subsequent coherent SAR images, it is possible to derive a map of the displacements along the sensor LOS from the obtained interferogram, with metric or sub-metric resolution, submillimeter accuracy and sampling frequency of few minutes (Tarchi et al., 1997, 2000; Rudolf et al., 1999; Pieraccini et al., 2000, 2002). The area covered by a GB-InSAR system depends on the distance between the sensor and the point of observation, but is usually limited to a minimum of a few hundred meters to a maximum of a few kilometers. According to the specific acquisition geometry, only this component of the real displacement vector can be estimated, whereas the displacements occurring along a direction perpendicular to the LOS are missed. This is the main limitation of the GB-InSAR technique. Given the favorable logistics and power supply, the installation viewpoint of the radar system must therefore be selected in order to make the sensor LOS as parallel as possible to the expected direction of the landslide motion. Nevertheless the GB-InSAR represents a versatile and flexible technology for landslide monitoring, allowing for rapid changes in the type of data acquisition, such as geometry and temporal sampling, based on the characteristics of the slope failure monitored (Antonello et al., 2004).

3.3. Terrestrial laser scanning

A TLS device measures the laser time-of-flight between the sensor and the reflecting targets with high accuracy (millimeter or centimeter). It can obtain the exact position of a mesh of points (point cloud), characterized by (x, y, z) Cartesian coordinates and the reflectance value $R(x, y, z)$, quickly providing a high-resolution 3D surface digital model of the scanned object (Slob et al., 2002; Frohlich and Mettenleiter, 2004; Slob and Hack, 2007). TLS is also used for analyzing unstable slopes to investigate the plano-altimetric morphological and geostructural setting of a rock mass, and is therefore suitable for rock cliff monitoring (Abellán et al., 2006, 2011; Turner et al., 2006; Slob and Hack, 2007; Teza et al., 2008; Ferrero et al., 2009; Oppikofer et al., 2009; Gigli et al., 2014). The high resolution of laser scanning permits the extraction of very small features such as the structural crack pattern, the crack opening direction (Gigli et al., 2009), and the orientation of critical discontinuities within the rock mass (Gigli and Casagli, 2011; Gigli et al., 2014). Furthermore, this technique is capable of measuring ground 3D temporal displacements by comparing sequential datasets (Rosser et al., 2005; Lim et al., 2006; Teza et al., 2008; Kasperski et al., 2010; Abellán et al., 2011).

3.4. Integrated monitoring system

Considering the variability of the instability processes affecting the San Leo rock plate, in terms of typology, velocity and location of the affected areas following the February 27th event, we planned a suitable monitoring system based on the synergic use of PS-InSAR and GB-InSARtechniques, coupled with TLS surveys (Fig. 4). A total of 74 SAR images, acquired with descending and ascending orbits by the Italian Space Agency (ASI) COSMO-SkyMed constellation of satellites, were used (Table 1). These satellites were chosen for their more innovative characteristics with respect to the other satellite missions, such as the use of microwave X-band, shorter revisiting time (in the order of a few days) and finer spatial resolution, effective for the rapid updating of landslide inventory maps and for hazard and risk studies. On March 7th 2014, a GB-InSAR system was installed

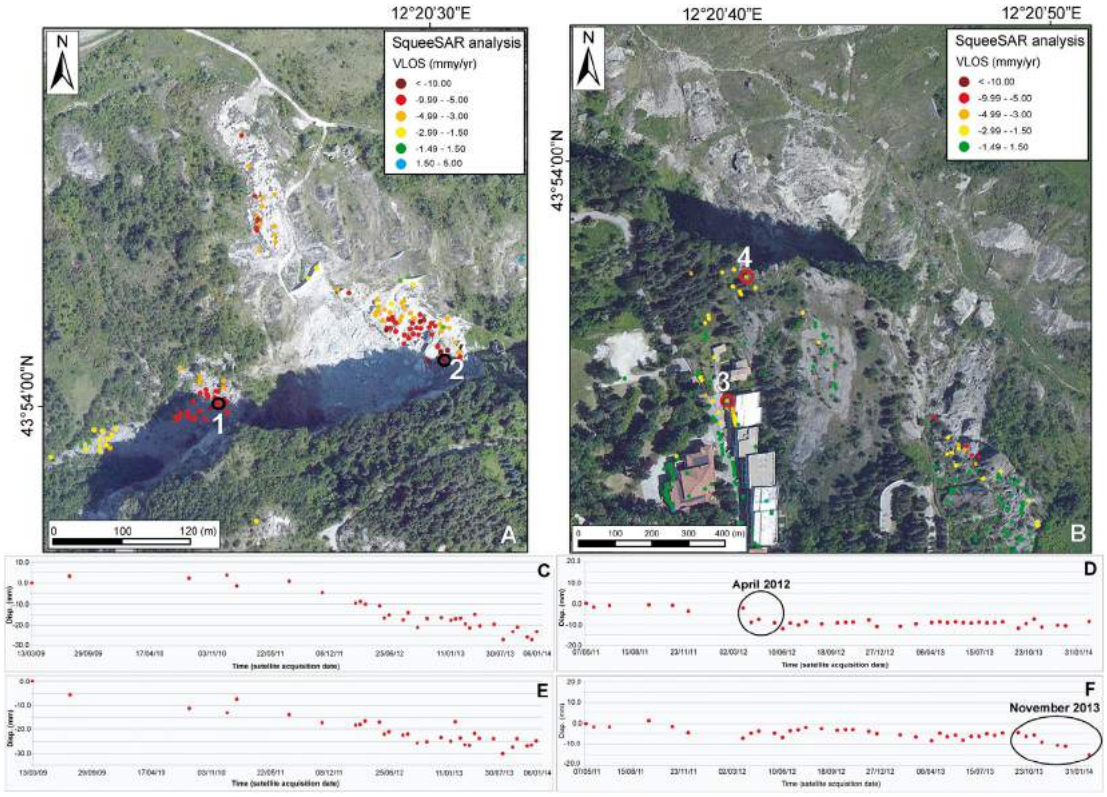

Fig. 7. Examples of COSMO-SkyMed velocity maps (areas 2 and 3 of Fig. 6A). (A) Descending geometry. (B) Ascending geometry. (C—F) Displacement time series of selected PSs for (C) point 1, (D) point 3, (E) point 2 and (F) point 4. Point locations are shown in A and B.

opposite to the north-eastern sector of the San Leo rock wall (Fig. 4A,C,D), for the real time monitoring of the residual movements of both the rock wall collapse-affected sector and the rock fall deposits. The employed radar system operates in the k_u-band (wavelength range of 2.5–1.67 cm; central frequency of 17.2 GHz and 200 MHz band width), and is capable of achieving a 3 m synthetic aperture in a 2 min scanning time. TLS surveys on the collapse-affected rock wall sector were carried out with a long range 3D laser scanner (RIEGL LMSZ410-I; Riegl, 2010). This device can determine the position of up to 12,000 points s^{-1} with a maximum angular resolution of 0.008° and an accuracy of ±10 mm from a maximum distance of 800 m. In order to completely cover the intervention areas, four different laser scanning surveys (07/03/2014, 09/04/2014, 11/06/2014 and 18/12/2014) were performed from different viewpoints (Fig. 5A,B). Several laser reflectors were placed in the surveyed area, and their coordinates were defined by performing a differential RTK-GPS survey, to link the different acquired point clouds to a global reference system. Riscan Pro 1.7.9 was the main software used for the visualization, alignment and comparison of the point clouds.

4. Results

4.1. PS-InSAR monitoring

Squee-SAR analysis was performed by using the X-band sensor COSMO-SkyMed images both in ascending and descending geometries (Table 1). Both the available datasets show a non-regular temporal acquisition which can lead to an incorrect evaluation of the ground deformation. This problem particularly affects the descending dataset for March 2000 to March 2012 in which only seven images were acquired. A more regular acquisition and the higher number of available images make the ascending dataset more reliable than the descending one.

Squee-SAR analysis using the ascending dataset highlighted ground deformation phenomena mainly located in correspondence of the rock plate bedrock, at the foot of the north-western, northern, and eastern rock plate bordering wall sectors (Fig. 6A,B). The more relevant displacements were detected in correspondence with rock blocks located northwestward of the 2014 rock fall. The highest detected velocities along the satellite LOS were -9.8 mm yr^{-1} (sector 2 in Fig. 6A) and 5.7 mm yr^{-1} (sector 1 in Fig. 6A). The rock blocks represents ancient rock fall deposits (Fig. 3A,B) as well as the 2006 rock fall and related deposits (Fig. 3A,D).

The ascending dataset includes displacements of ancient rock fall deposits (Fig. 3A,C) at the foot of the rock plate eastern sector, below the medieval fortress, where the highest detected velocity along the satellite LOS was -8.7 mm yr^{-1} (Fig. 6A). PSs record the sliding of single blocks after the 2006 rock fall event, which moved the underlying ductile materials downslope as an earth flow (Fig. 6C). Even though the descending dataset is less reliable than the ascending one, it clearly shows the ground deformation at the northern toe of the cliff (Fig. 6A,B), in correspondence with the 2006 rock fall and earth flow deposits (Fig. 3A,D). In this case the registered velocities range between -3.0 and -20.0 mm yr^{-1}. The ascending dataset shows the presence of an area located on the rock plate, in the northern sector of the town, along the cliff affected by the 2014 rock fall (Fig. 6A,B). Here the deformation velocities are notably lower than those observed for the deposits, nevertheless PSs highlight that the area is affected by deformation. In this sector velocities along the LOS range between -4.9 and -1.7 mm yr^{-1}. The southern and central parts of the rock plate show an overall stability. Most of the PSs located in these areas are characterized by velocities comprised in the stability range.

The projection of the velocity of each of PS along the slope is a procedure that leads to a better evaluation of the real magnitude of the velocity, because it is evaluated along the dip of the slope instead of along the satellite LOS. A drawback of this approach is a decrease in the PSs number because Ps with positive velocity are discarded (Notti et al., 2014). In this case the decrease of PS population is 47% for the ascending dataset and 16% for the descending one.

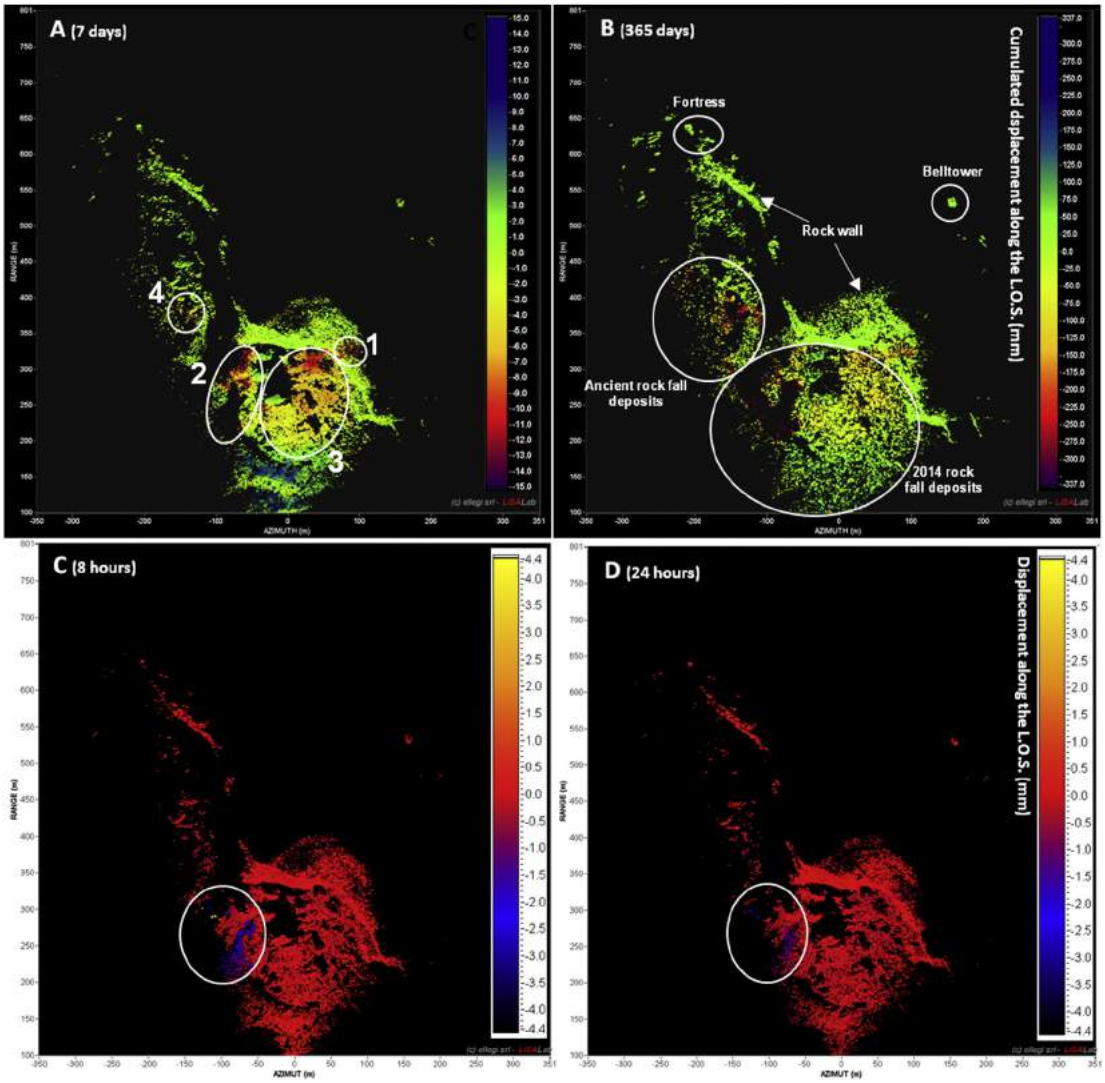

Fig. 8. GB-InSAR displacement maps of the San Leo 2014 rock fall deposit and north-eastern rock wall sector. (A) Cumulated displacement measured from March 7th to 15th, 2014, and detected critical sectors (1–4). (B) Cumulated displacement map measured for March 7th 2014 to March 7th 2015. (C) Displacement map between 04:00 and 12:00, June 18th 2014. D) Displacement map between 12:00 August 25th and 12:00 August 26th, 2014. Ovals in C and D show the sectors of rock fall deposit characterized by higher displacements.

Despite such decrease, some interesting results can be observed: the ascending dataset continues to highlight the presence of ground deformations in the same areas previously detected. The V_{slope} velocities at the northwestern sector of the cliff affected by the 2014 rock fall range between 5 and 9 mm yr^{-1} which are almost twice those measured along the LOS (Fig. 6C). The highest V_{slope} values are detected in correspondence with the blocks located at the northwestern toe of the cliff, where the calculated V_{slope} velocities reach 33.9 mm yr^{-1}.

The descending dataset confirms the deformation in this area but does not reveal the presence of ground deformation along the cliff (Fig. 6D). The time series analysis of the ascending dataset includes the possible precursory phenomena of the 2014 rock fall (Fig. 7A). In particular the time series of several PSs located along the northeastern sector of the cliff show that during April 2012 and November 2013 there were two phases of increased deformation velocity (Fig. 7C,D) with respect to the stable trend recorded in the rest of the analyzed period. Time series analysis of deposits produced by the 2006 landslide event shows a more linear trend (Fig. 7B), confirming that the blocks produced by the less recent events are affected by a continuous deformation still ongoing after 9 years.

4.2. GB-InSAR monitoring

The fast sampling frequency of the GB-InSAR system allowed us to produce interferograms covering different time periods (11 min and 2, 8, and 24 h) and cumulated displacement maps of selectable time spans (Fig. 8). The first radar images proved the system capability to display: i) a portion of the fortress walls; ii) the abbey church bell tower; iii) the rock wall collapse-affected sector; iii) the 2014 rock fall deposits; and iv) ancient rock fall deposits. The GB-InSAR data acquired during the first monitoring week allowed us to assess a relative stability of the rock cliff and the town structures observed, and to detect four main critical areas (Figs. 8A and 9). Sector 1 is characterized by 17 mm maximum cumulative displacement, which corresponds to a detensioned rock block located at the foot of the monitored rock wall central sector (Fig. 9A,C). Sector 2 displays a maximum cumulative displacement of 14 mm, located at a collapsed deca-metric rock block, completely detached from the rock wall (Fig. 9A,D). Sector 3 shows cumulative displacements ranging 4 to 11 mm, at the main portion of the rock fall deposits with metric-size boulders to blocks in a coarse sandy-clayey matrix (Fig. 9A,E). Sector 4 corresponds to ancient rock fall deposits (Fig.4 A,C), characterized by 12 mm of maximum cumulative displacements (Fig. 9A). At the end of the GB-InSAR monitoring period examined, the maximum recorded cumulative

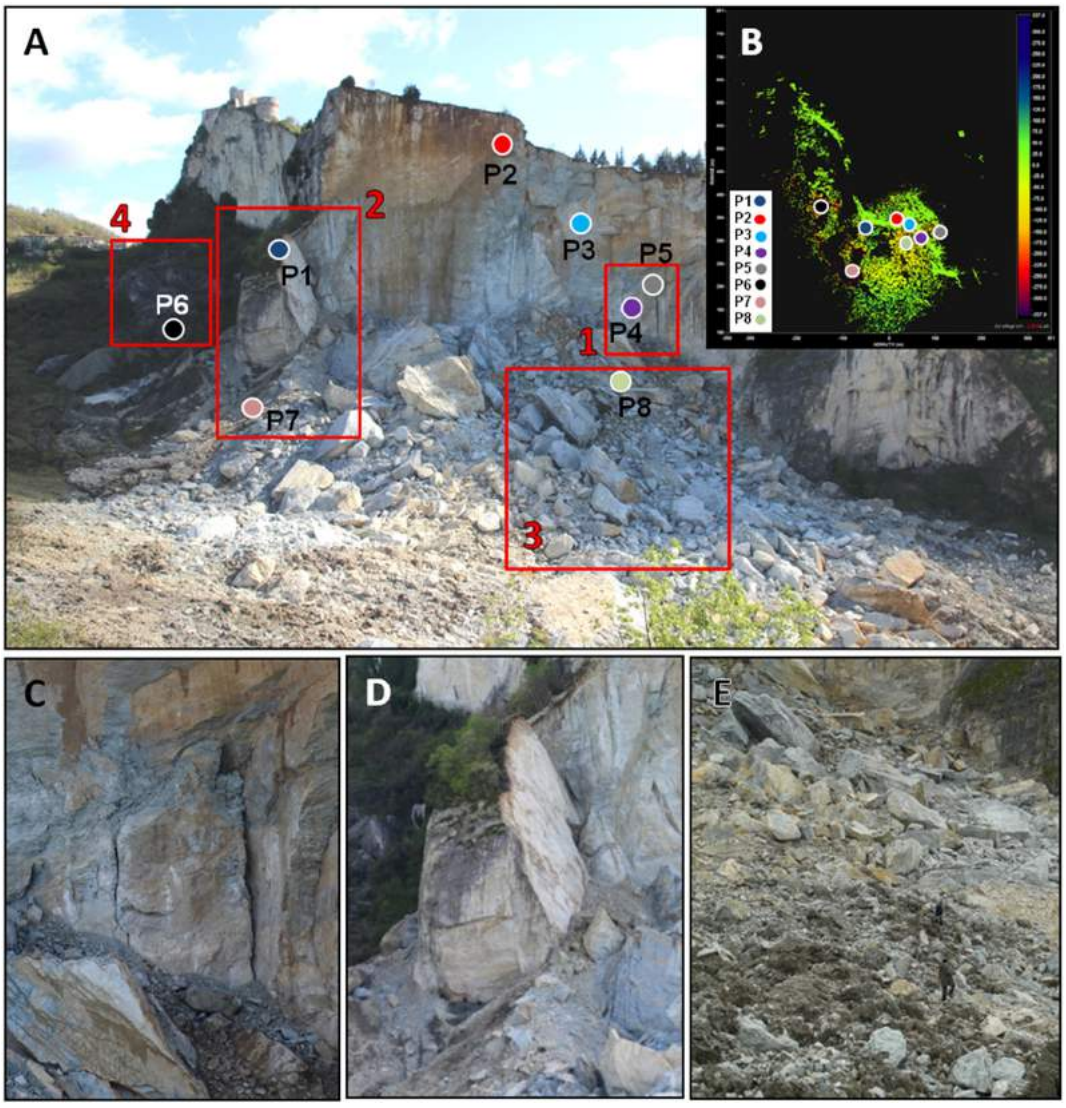

Fig. 9. Field pictures. (A) Monitored rock wall. (B) Related GB-InSAR monitoring control points P1–P8. Red open squares in (A) show the detected four critical areas (sectors 1 to 4). (C) sector 1. (D) sector 2. (E) sector 3. Sector 4 is shown in Fig. 3C.

displacement in the investigated area is 339 mm, corresponding to the rock fall deposits surrounding the above-mentioned deca-metric rock block in sector 2, whereas in sectors 1, 3 and 4, it reaches 270, 180 and 230 mm, respectively (Fig. 8B). Most of the rock wall, as well as the fortress and the abbey church bell tower, were generally stable. From the start of the monitoring period, the highest daily cumulative displacements (3–4 mm day^{-1}) were constantly recorded at sector 2 (Figs. 8A,C,D and 9A,D), whereas on June 18th 2014, the peak daily displacements of about 15 mm occurred (Fig. 8C). In order to assess the kinematics of the rock wall and rock fall deposits, eight control points were selected (Fig. 9A,B) and their displacement time series up to March 7th, 2015 was extracted and analyzed (Fig. 10): P1 and P7 located at sector 2 (Figs. 8A and 9A,B,D); P2 and P3 at stable rock wall sectors; P4 and P5 at sector 1 (Figs. 8A and 9A,B,C); P6 at sector; and P8 at sector 3 (Figs. 8A and 9A,B,E). Cumulated displacements range from 108 mm at P1 to 339 mm at P7. On the basis of the kinematic behavior of the control points, seven acceleration events were detected (Fig. 10).

Analysis of the displacement time series of the selected control points indicated that P2 and P3, corresponding to stable rock wall sectors, show a general stability for the entire period monitored (March 7th 2014 to March 7th 2015). P6, located on ancient rock fall deposits below the Fortress, is characterized by a linear deformation trend with a 0.6 mm day^{-1} mean rate. Analysis of P1, P4, P5 and P8 displacement time series shows relatively constant movements over time with an average speed of about 0.3 mm day^{-1} for P1 and P4, 0.8 mm day^{-1} for P5 and 0.5 mm day^{-1} for P8 (Table 2). This kinematic continuity was interrupted

Table 2
Cumulated displacements of P1–P4–P5–P8 GB-InSAR control points (in mm) and acceleration events with mean velocity in mm day^{-1}.

Time period	Elapsed days	P1 displacement (velocity)	P4 displacement (velocity)	P5 displacement (velocity)	P8 displacement (velocity)
07/03/2014–07/03/2015	365	108.5 (0.3)	113.9 (0.3)	281.1 (0.8)	172.9 (0.5)
25/03/2014–13/04/2014	19	43.5 (2.3)	15.7 (0.8)	36.7 (1.9)	27 (1.4)
27/04/2015–15/05/2014	18	18.9 (1.0)	13.4 (0.7)	33.1 (1.8)	30.9 (1.7)
01/12/2014–06/12/2014	5	2.3 (0.5)	3.2 (0.6)	4.3 (0.9)	2.8 (0.6)

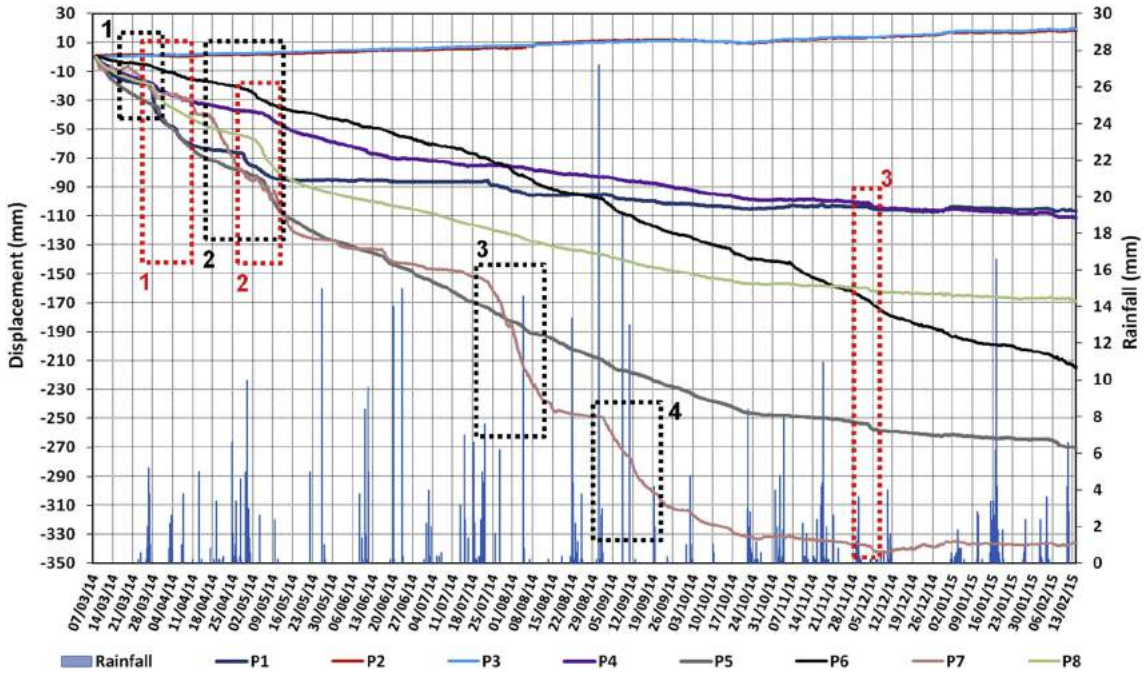

Fig. 10. Displacement time series of the selected GB-InSAR control points (P1–P8) and daily rainfall data. Red dotted open squares highlight acceleration events of P1, P4, P5, and P8; black dotted open squares show acceleration events of P7.

by three accelerations: the first from March 25th to April 13th, 2014; the second from April 27th to May 15th, 2014; the third from December 1st to 6th, 2014.

P7, located on the 2014 rock fall deposits, shows the highest deformation in terms of both velocity (about 1 mm day^{-1}) and cumulated displacement (339 mm year^{-1}). Moreover, four acceleration periods were detected: March 18th to 29th, 2014; April 15th to May 15th, 2014; July 21st to August 15th, 2014; and August 31st to September 25th, 2014 (Table 3).

4.3. TLS surveys

The acquired discrete point clouds of the analyzed rock wall were merged using triangulation into a continuous 3D terrain model

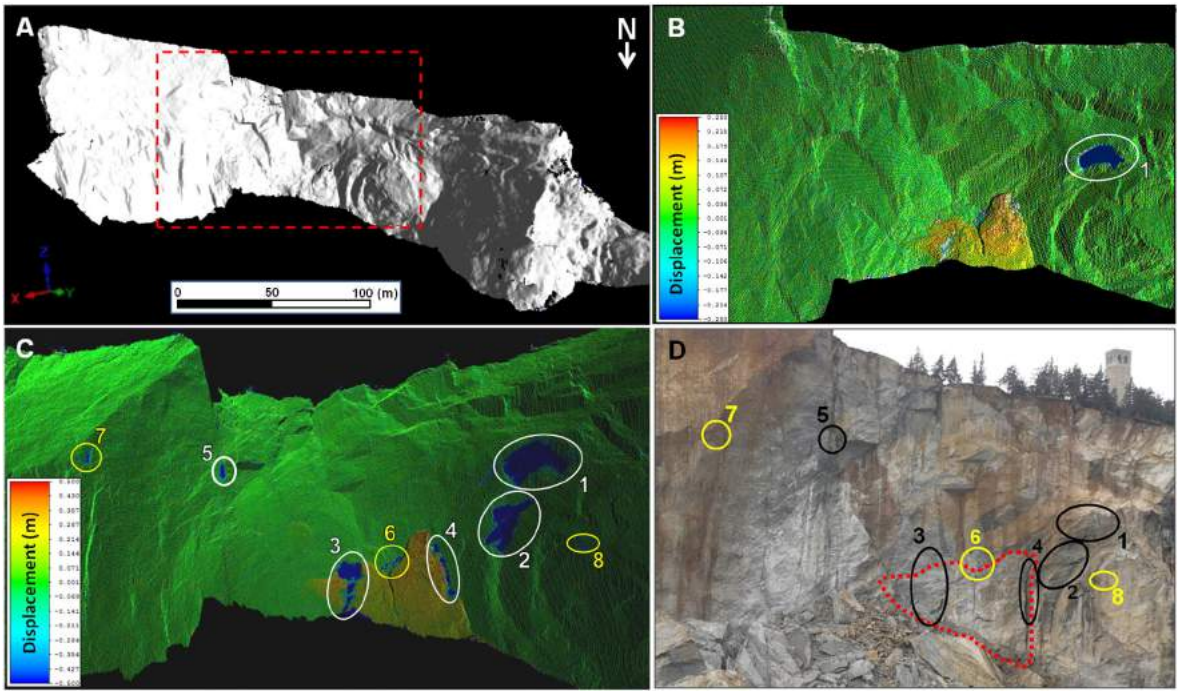

Fig. 11. TLS survey results. (A) High resolution 3D surface of the surveyed rock wall. Red dashed open square corresponds to the area affected by rock block detachments in Fig. 11B,C. (B) Comparison between March 7th and April 9th scans showing the first monitored rock block detachment (blue area in white oval 1). and the rock wall sector characterized by displacements (orange-yellow areas). (C) Comparison between March 7th and December 18th scans, showing detached rock block sectors in blue (white ovals show larger events and yellow ovals show smaller ones) and the rock wall sector characterized by displacements (orange-yellow areas). (D) Correspondent sectors in the optical image; red dotted line delimits the rock wall displaced sector.

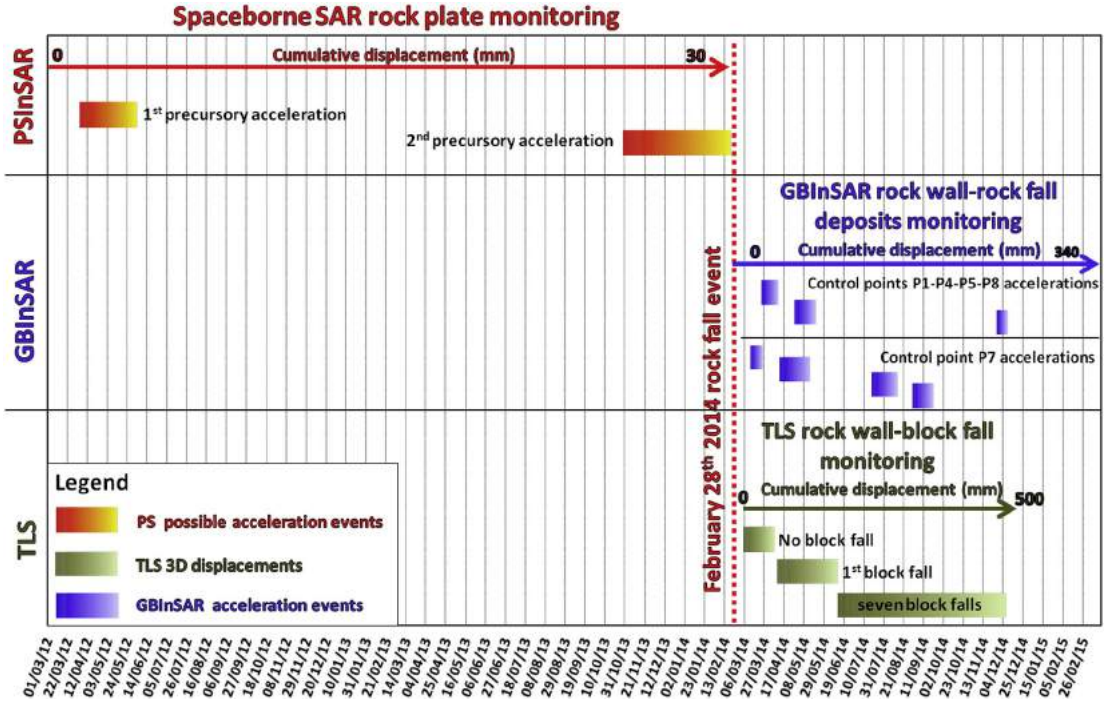

Fig. 12. Monitoring time line of the employed systems.

(Fig. 11A). It revealed a rough rock wall surface, characterized by overhanging sectors, ledges and niches. Temporal variations of terrain were detected by comparing sequential datasets from different laser scanning surveys, as performed by Rosser et al. (2005) and Lim et al. (2006). For evaluating the total strain field of the rock wall, the four scanning results were compared; the resulting temporal variations from March 7th to December 18th, 2014, are shown in Fig. 11C. For each scanned point the displacement vector was determined perpendicularly to the former local surface. The deformational field analysis indicated an ongoing rock block toppling with an estimated volume of 450 m^3, which is almost completely detached from the central sector of the rock wall (Fig. 11B,C). The displacement since March 7th was 12 cm on April 9th, 25 cm on June 11th and about 50 cm on December 18th (Fig. 11C). The detachment of rock blocks occurred frequently but with the lowest magnitude among all mass movements. The scan comparison also revealed block fall (blue areas in Fig. 10B,C). The volume of rock blocks and the period when they detached are shown in Table 4. The major rock block detachment occurred during April 9th to June 11th, involving a 94 m^3 rock volume, whereas the rest took place during June 11th to December 18th, involving minor detachments from 66 to 1 m^3 in volume. Thus, based on their volume, the block falls were subdivided into major (94–10 m^3) and minor (1–2 m^3) ones.

5. Discussion

Space-borne InSAR can be used to detect ground deformation both on a local scale and over large areas and it is suitable for detection and/or monitoring phenomena with low velocity (Meisina et al., 2008). The PS-InSAR technique allowed a preliminary study on the generalized rock mass stability and slow ground displacements, to detect and monitor possible precursory phenomena highlighted by local accelerations in PS time series (Fig. 12). Rock falls including those occurring in San Leo are usually characterized by fast velocities reducing the suitability of space-borne InSAR methodologies. SAR data do not allow the measurement of deformations faster than a few tens of cm per year, because aliasing effects limits the maximum detectable displacement to a quarter of the radar wavelength (Hanssen, 2005; Crosetto et al., 2010). For example, 68 cm yr^{-1} is the maximum velocity detectable by using the COSMO-SkyMed system with four operating satellites in X band. In addition, the spatial coverage of satellite images is limited by the peculiar SAR imaging geometry, with large mountainous areas masked by foreshortening, layover and shadowing effects. The area located along the northern side of the San Leo rock plate is partly affected by these geometric distortions which along with the presence of vegetation reduced the number of available PSs. These problems have been partly solved in this study using the GB-InSAR system, as its versatility also allows placing the device in front of steep slopes, which are in most cases not visible from space-borne platforms. Furthermore, faster sampling frequency of the GB-InSAR system makes this technique suitable for monitoring short term slope movements (Corsini et al., 2006; Noferini et al., 2007), such as the possible displacement of the rock wall collapsed-affected sector and residual movements of rock fall deposits. The analysis of the time series of the GB-InSAR control points also allowed us to investigate the kinematics of deposits from the 2014 rock fall event (Fig. 10), detecting seven acceleration events (Tables 2 and 3; Fig. 12). Acceleration of control point P7 seems to be driven by major precipitation events (Fig. 10).

TLS does not suffer from some problems associated with GB-InSAR such as loss of coherence, decorrelation, and displacement detection capability only along the LOS of the instrument. On the other hand, GB-InSAR single measures can reach submillimeter accuracy, while TLS is not suitable to detect displacements smaller than 10 mm (Pratesi et al., 2015). TLS is suitable for assessing minor rock fall events on a cliff, which are too fast to be detected by the GB-InSAR system (Figs. 11 and 12; Table 4). Furthermore the TLS model was merged with the GB-InSAR data to obtain a 3D GB-InSAR cumulative

Table 3
Cumulated displacements of P7 control point (in mm) and acceleration events with mean velocity in mm day^{-1}.

Time period	Elapsed days	P 7 displacement (velocity)
07/03/2014–07/03/2015	365	339.1 (0.9)
18/03/2014–29/03/2014	11	19.9 (1.8)
15/04/2015–15/05/2014	31	78.5 (2.5)
21/07/2014–15/08/2014	25	91.0 (3.6)
31/08/2014–25/09/2014	25	62.6 (2.5)

Table 4
Detected detached blocks and their calculated volumes.

Detached sector	Calculated volume (m^3)	Time interval (2014)
1	94	April 9th–June 11th
2	66	June 11th–December 18th
3	44	
4	15	
5	10	
6	2	
7	1.5	
8	1	

displacement map, which allowed us to read detected LOS displacements directly on the observed 3D representation scenario, and therefore to better localize the most critical areas (Fig. 13A). The accuracy in locating a GB-InSAR control point is affected by the system azimuth and range resolutions, which are related to the distance between the sensor and the backscattering objects. Regarding the San Leo case study, the investigated rock wall has a subvertical geometry which in some portions shows overhanging sectors (Fig. 13B). In this framework, the GB-InSAR system installation associated with the surveyed scenario, leads to a different range resolution of scenario sectors located at different heights along the surveyed rock wall. The 3D displacement map obtained (Fig. 13A) shows an ambiguity in locating deformation sectors along the rock wall. Therefore, in this specific case study sectors characterized by displacements are displayed as vertical zones instead of pixel clusters located at the cliff bottom (Fig. 11C). The 3D GB-InSAR displacement map was also used for a comparison between TLS and GB-InSAR displacement data. The difference in the recorded displacements detected by the two monitoring systems at sector 1 (Figs. 8 and 9), is related to the different displacement components of the recorded movements, because the two monitoring systems have different LOSs.

6. Conclusions

On February 27th 2014, an entire portion of the rock massif, on which the historic town of San Leo is located, collapsed and caused a huge rock fall. To monitor the ground deformation afterwards and assess the residual risk of landslide displacements, a monitoring system based on remote sensing techniques including radar interferometry (PS-InSAR and GB-InSAR) and terrestrial laser scanning was established. The PS-InSAR technique, by using archival SAR images, allowed us to analyse pre- and a post-event displacements, rock massif stability, and the residual movements of the San Leo rock plate (Figs. 3, 6, 7, and 8A). It facilitated detection of possible precursory phenomena highlighted by local accelerations in the PSs time series (Fig. 12). The GB-InSAR one year monitoring campaign from March 7th 2014 to March 7th 2015 allowed analysis of the short-term behavior of deposits from the 2014 rock fall event. General stability of the monitored structures (fortress walls and abbey church bell tower) and the main portion of the rock wall was assessed. Based on the recorded cumulative displacement values, four critical sectors were detected: 1) a collapse-affected rock wall completely detached from the stable portions (Figs. 8A and 9A,B,C); 2) a collapsed deca-metric rock block, completely detached from the rock wall (Figs. 8A and 9A,B,D), where the maximum cumulative displacement in the monitored area (339 mm) was recorded; 3) the main portion of the 2014 rock fall deposits (Figs. 8A and 9E); and 4) ancient rock fall deposits (Figs. 3A,C, 6, and 7). In order to assess the kinematics of the rock wall and rock fall deposits, eight control points (from P1 to P8) were selected (Fig. 9) and their displacement time series up to March 7th, 2015 analyzed (Fig. 10, Tables 2 and 3). Seven acceleration events were detected, and those related to P7 are correlated with rainfall events (Figs. 10 and 12). TLS data provided high resolution 3D data for a rough rock wall surface, characterized by criticalities such as overhanging sectors, ledges and niches (Fig. 11A). 3D temporal variations of the terrain model were detected by comparing sequential datasets acquired from different laser scanning surveys, from March 7th to December 18th, 2014 (Figs. 11 and 12, Table 4). It provided evidence of an ongoing rock block toppling at sector 1 detected through the GB-InSAR monitoring (Figs. 8A and 9A,B,C), and identified seven distinct block falls with their volume. The San Leo area is characterized by complex geomorphological features, different ongoing landslide processes with various states of activity. Each single monitoring technique is inadequate for its intrinsic limitations, but the combined use of the techniques provided an effective monitoring system of landslide activity, thanks

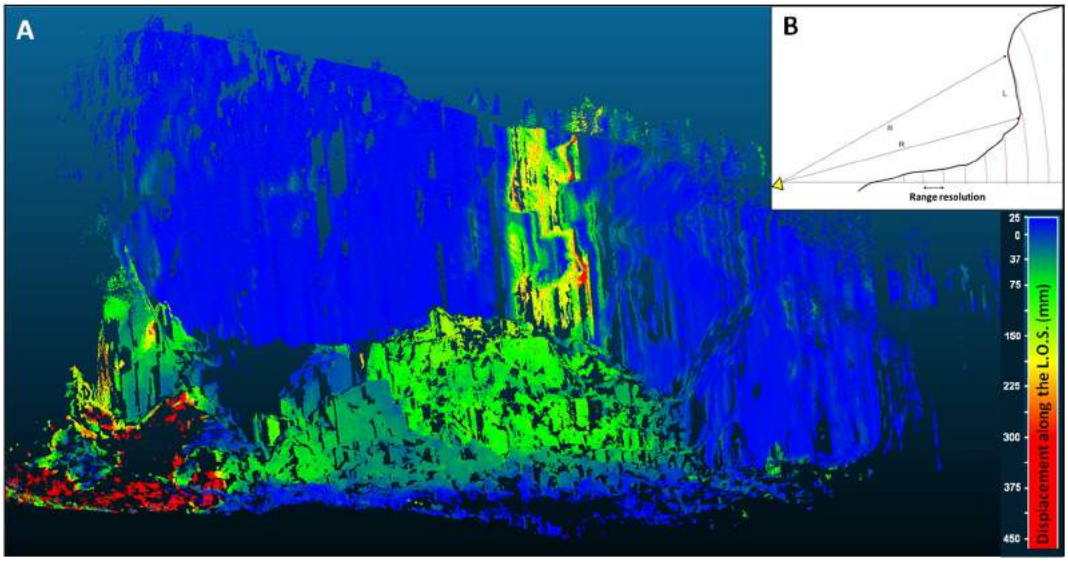

Fig. 13. GB-InSAR and TLS data integration. (A) 3D GB-InSAR cumulative displacement map of the San Leo rock wall. In the central sectors the area characterized by deformation ambiguity is clearly visible. (B) Simplified sketch of the rock wall geometry. R: distance sensor-target. L: length of rock wall overhanging sectors.

to the different instrument characteristics in relation to LOS, range of detectable velocity, and repetition time.

Acknowledgements

The GB-InSAR apparatus used was designed and produced by Ellegi s.r.l., and based on the proprietary technology GB-InSAR LiSALAB provided through the improvement of LiSA technology licensed to the Ispra Joint Research Centre of the European Commission. The available pre-event COSMO-SkyMed data were processed by Tele-Rilevamento Europa (TRE).

References

Abellán, A., Vilaplana, J.M., Martínez, J., 2006. Application of a long-range terrestrial laser scanner to a detailed rockfall study at Vall de Núria (eastern pyrenees, Spain). Eng. Geol. 88, 136–148.

Abellán, A., Vilaplana, J.M., Calvet, J., Garcıa-Selles, D., Asensio, E., 2011. Rockfall monitoring by terrestrial laser scanning — case study of the basaltic rock face at Castellfollit de la Roca (Catalonia, Spain). Nat. Hazards Earth Syst. Sci. 11, 829–841.

Al-kheder, S., Al-shawabkeh, Y., Haala, N., 2009. Developing a documentation system for desert palaces in Jordan using 3-D laser scanning and digital photogrammetry. J. Archaeol. Sci. 36, 537–546.

Antonello, G., Casagli, N., Farina, P., Leva, D., Nico, G., Sieber, A.J., Tarchi, D., 2004. Ground based SAR interferometry for monitoring mass movements. Landslide 1, 21–28.

Arayici, Y., 2007. An approach for real world data modelling with the 3-D terrestrial laser scanner for built environment. Autom. Constr. 16, 816–829.

Bamler, R., Hartl, P., 1998. Synthetic aperture radar interferometry. Inverse Probl. 14, 1–54.

Bardi, F., Frodella, W., Ciampalini, A., Bianchini, S., Del Ventisette, C., Gigli, G., Fanti, R., Moretti, S., Basile, G., Casagli, N., 2014. Integration between ground based and satellite SAR data in landslide mapping: The San Fratello case study. Geomorphology 223, 45–60.

Bellotti, M., Bianchi, D., Colombo, A., Ferretti, A. Tamburini, 2014. Advanced InSAR techniques to support landslide monitoring. In: Pardo-Igúzquiza, E., Guardiola-Albert, C., Heredia, J., Moreno-Merino, L., Durán, J.J., Vargas-Guzmán, J.A. (Eds.), Mathematics of Planet EarthLecture Notes in Earth System Sciences. Springer, Berlin Heidelberg, pp. 287–290.

Benedetti, G., Bernardi, M., Borgatti, L., Continelli, F., Ghirotti, M., Guerra, C., Landuzzi, A., Lucente, C.C., Marchi, G., 2013. San Leo: centuries of coexistence with landslides. In: Margottini, C., Canuti, P., Sassa, K. (Eds.), Landslide Science and Practice. Springer, Heidelberg, Germany, pp. 529–537.

Bertocci, R., Canuti, P., Casagli, N., Garzonio, C.A., 1991. Deep seated gravitational slope deformations and landslides in north-Central Italy: geotechnical analyses, mechanisms and evolutive models of the phenomena. Proc. of the International Symposium on Landslide and Geotechnics (ISLG), 13–20, Wuhan, China, May 1991.

Bianchini, S., Ciampalini, A., Raspini, F., Bardi, F., Di Traglia, F., Moretti, S., Casagli, N., 2014. Multi-temporal evaluation of landslide movements and impacts on buildings in San Fratello (Italy) by means of *C*-band and X-band PSI data. Pure Appl. Geophys. http://dx.doi.org/10.1007/s00024-014-0839-2.

Bianchini, S., Pratesi, F., Nolesini, T., Casagli, N., 2015. Building deformation assessment by means of persistent scatterer interferometry analysis on a landslide-affected area: the Volterra (Italy) case study. Remote Sens. 7, 4678–4701.

Boehler, W., Heinz, G., Marbs, A., 2001. The potential of non-contact close range laser scanners for cultural heritage recording. Proceedings of the 18th International Symposium of CIPA, Potsdam, Germany, pp. 18–21.

Borgatti, L., Guerra, C., Nesci, O., Romeo, R.W., Veneri, F., Landuzzi, A., Benedetti, G., Marchi, G., Lucente, C.C., 2015. The 27 february 2014 San Leo landslide (Northern Italy). Landslides 12, 387–394.

Broussolle, J., Kyovtorov, V., Basso, M., Ferraro Di Silvi, E., Castiglione, G., Figueiredo, Morgado, J., Giuliani, R., Oliveri, F., Sammartino, P.F., Tarchi, D., 2014. MELISSA, a new class of ground based InSAR system. An example of application in support to the Costa Concordia. ISPRS J. Photogramm. Remote Sens. 91, 50–58.

Bűrgmann, R., Hilley, G., Ferretti, A., Novali, F., 2005. Resolving vertical tectonics in the San Francisco Bay area from permanent scatterer InSAR and GPS analysis. Geology 34, 221–224.

Cancelli, A., Pellegrini, M., 1987. Deep seated gravitational deformations in the northern Apennines, Italy. Proc. 5th ICFL, Australia and New England, 1–8, August 1987.

Canuti, P., Casagli, N., Garzonio, C.A., Vannocci, P., 1990. Lateral spreads and landslide hazards in the northern Apennine: the example of the Mt. Fumaiolo (Emilia-Romagna) and Chiusi della Verna (Tuscany). Proceedings 6th Congr. IAEG, Amsterdam, 3, pp. 1525–1533.

Canuti, P., Casagli, N., Garzonio, C.A., 1999. Slope instability at a historical site, La Verna monastery, Italy. In: Sassa, K. (Ed.), Landslides of the World, Kyoto, Japan Landslide Society. Kyoto University Press, pp. 348–352.

Canuti, P., Casagli, N., Ermini, L., Fanti, R., Farina, P., 2004. Landslide activity as a geoindicator in Italy: significance and new perspectives from remote sensing. Environ. Geol. 45, 907–919.

Casagli, N., Focardi, P., Garduño, H., Garzonio, C.A., Tarchiani, U., Vannocci, P., 1994. Large-scale complex slope movements at Sasso di Simone-Mt Simoncello. Mem. Soc. Geol. Ital. 48, 873–880.

Caturani, A., Ribacchi, R., Tommasi, P., 1991. The San Leo Cliff (Italy): stability conditions and remedial measures. VII ISRM Int. Congr. On Rock Mechanics, Aachen Vol. 2, pp. 853–858.

Cestelli-Guidi, C., Croci, G., and Ventura, P., 1984. Stability of the Orvieto rock. In: Proc 5th Congress of the International Society for Rock Mechanics, Melbourne, 10–15 April 1983, V1, PC31–C38. Publ Rotterdam: A. A. Balkema, 1983, Int. J. Rock Mech. Min. Abstr. Vol. 21, (152 pp.)

Ciampalini, A., Cigna, F., Del Ventisette, C., Moretti, S., Liguori, V., Casagli, N., 2012. Integrated geomorphological mapping in the north-western sector of Agrigento (Italy). J. Maps 8, 136–145.

Ciampalini, A., Bardi, F., Bianchini, S., Frodella, W., Del Ventisette, C., Moretti, S., Casagli, N., 2014. Analysis of building deformation in landslide area using multisensor PSInSAR™ technique. Int. J. Appl. Earth Obs. Geoinf. 33, 166–180.

Conti, S., 1989. Geologia dell'Appennino marchigiano romagnolo tra le valli del Savio e del Foglia (Note illustrative alla carta geologica a scala 1:50.000). Boll. Soc. Geol. It. 108, 453–490.

Conti, S., 2002. Palaeogeographic implications and relations between tectonics and sedimentation in satellite basins (northern Apennines): insights from Neogene Epiligurian arcs. Bollettino Della Societa` Geologica Italiana Vol. Volume Speciale 1, pp. 353–364.

Conti, S., Tosatti, G., 1996. Tectonic vs gravitational processes affecting Ligurian and Epiligurian units in the Marecchia valley (northern Apennines). Mem. Sci. Geol. 48, 107–142.

Cornamusini, G., Conti, P., Bonciani, F., Callegari, I., Carmignani, L., Martelli, L., Quagliere, S., 2010. Note illustrative della carta Geologica d'Italia. Foglio 267 San Marino, scala 1: 50.000 (pp. 125). Roma: ISPRA.

Corsini, A., Farina, P., Antonello, G., Barbieri, M., Casagli, N., Coren, F., Guerri, L., Ronchetti, F., Sterzai, P., Tarchi, D., 2006. Space-borne and ground-based SAR interferometry as tools for landslide hazard management in civil protection. Int. J. Remote Sens. 27, 2351–2369.

Costantini, M., Iodice, A., Magnapane, L., Pietranera, L., 2000. Monitoring terrainmovements by means of sparse SAR differential interferometric measurements. Proc. IGAARSS, Honolulu, USA, pp. 3225–3227.

Cotecchia, V., 1997. Geotechnical degradation of the archaeological site of Agrigento. In: Viggiani, C. (Ed.), Proc. Int. Symposium on Geotechnical Engineering for the Preservation of Monuments and Historic Sites. A.A.Balkema, Rotterdam, pp. 101–108.

Crosetto, M., Monserrat, O., Iglesias, R., Crippa, B., 2010. Persistent scatterer interferometry: Potential, limits and initial *C*– and X-band comparison. Photogramm. Eng. Remote. Sens. 76, 1061–1069.

Cruden, D.M., Varnes, D.J., 1996. Landslide types and processes. In: Turner, A.K., Schuster, R.L. (Eds.), Landslides: Investigation and Mitigation, Sp. Rep. 247, Transportation Research Board, National Research Council.National Academy Press, Washington DC, pp. 36–75

De Capoa, P., D'Errico, M., Di Staso, A., Perrone, V., Perrotta, S., Tiberi, V., 2015. The succession of the val Marecchia Nappe (northern Apennines, Italy) in the light of new field and biostratigraphic data. Swiss J. Geosci. (in press).

De Feyter, A.J., 1991. Gravity tectonics and sedimentation of the Montefeltro (Italy). Geol. Ultraiect. 35, 1–168.

Del Ventisette, C., Ciampalini, A., Manunta, M., Calò, F., Paglia, L., Ardizzone, F., Mondini, A.C., Reichembach, P., Mateos, R.M., Bianchini, S., Garcia, I., Füsi, B., Deak, Z.V., Radi, K., Graniczny, M., Kowalski, Z., Piatkowska, A., Przylucka, M., Retzo, H., Strozzi, T., Colombo, D., Mora, O., Sanches, F., Herrera, G., Moretti, S., Casagli, S., Guzzetti, F., 2013. Exploitation of large archives of ERS and ENVISAT *C*-band SAR data to characterize ground deformations. Remote Sens. 5 (8), 3896–3917.

Delmonaco, G., Leoni, G., Margottini, C., Spizichino, D., 2015. Implementation of advanced monitoring system network in the Siq of Petra (Jordan). In: Lollino, G., Giordan, D., Marunteanu, C., Christaras, B., Yoshinori, I., Margottini, C. (Eds.), Engineering Geology for Society and Territory Vol. Volume 8. Springer International Publishing, pp. 299–303.

Di Traglia, F., Intrieri, E., Nolesini, T., Bardi, F., Del Ventisette, C., Ferrigno, F., Frangioni, S., Frodella, W., Giglio, G., Lotti, A., Tacconi Stefanelli, C., Tanteri, L., Leva, D., Casagli, N., 2014. The ground-based InSAR monitoring system at Stromboli volcano: Linking changes in displacement rate and intensity of persistent volcanic activity. Bull. Volcanol. 76, 1–18.

Egglezos, D., Moullou, D., Mavromati, D., 2008. Geostructural analysis of the Athenian acropolis wall based on terrestrial laser scanning data. The International Archives of the Photogrammetry Remote Sensing and Spatial Information Sciences, 37, B5, Beijing.

Fanti, R., Gigli, G., Lombardi, L., Tapete, D., Canuti, P., 2013. Terrestrial laser scanning for rockfall stability in the cultural heritage site of Pitigliano (Italy). Landslides 10, 409–420.

Ferrero, A.M., Forlani, G., Roncella, R., Voyat, H.I., 2009. Advanced geostructural survey methods applied to rock mass characterization. Rock Mech. Rock. Eng. 42, 631–665.

Ferretti, A., Prati, C., Rocca, F., 2000. Non-linear subsidence rate estimation using permanent scatterers in differential SAR interferometry. IEEE Trans. Geosci. Remote Sens. 38, 2202–2212.

Ferretti, A., Prati, C., Rocca, F., 2001. Permanent scatterers InSAR interferometry. IEEE Trans. Geosci. Remote Sens. 39 (1), 8–20.

Ferretti, A., Bianchi, M., Prati, C., Rocca, F., 2005. Higher-order permanent scatterers analysis. Eurasip J. Appl. Signal Process. 20, 3231–3242.

Frohlich, C., Mettenleiter, M., 2004. Terrestrial laser scanning: new perspectives in 3D surveying. In: Thies, M., Koch, B., Spiecker, H., Weinacker, H. (Eds.), Laser Scanners for Forest and Landscape Assessment, 36. International Archives of Photogrammetry, Remote Sensing and Spatial Information Sciences; P.8/W2.

Giardino, M., Mortara, G., Borgatti, L., Nesci, O., Guerra, C., Lucente, C.C., 2015. Dynamic geomorphology and historical iconography. Contributions to the knowledge of environmental changes and slope instabilities in the Apennines and the alps. In: Lollino,

G., Giordan, D., Marunteanu, C., Christaras, B., Yoshinori, I., Margottini, C. (Eds.), I, Engineering Geology for Society and Territory Vol. Volume 8. Springer International Publishing, pp. 463–468.
Gigli, G., Casagli, N., 2011. Semi-automatic extraction of rock mass structural data from high resolution LIDAR point clouds. Int. J. Rock Mech. Min. Sci. 48, 187–198.
Gigli, G., Mugnai, F., Leoni, L., Casagli, N., 2009. Analysis of deformations in historic urban areas using terrestrial laser scanning. Nat. Hazards Earth Syst. Sci. 9, 1759–1761.
Gigli, G., Frodella, W., Mugnai, F., Tapete, D., Cigna, F., Fanti, R., Intrieri, E., Lombardi, L., 2012. Instability mechanisms affecting cultural heritage sites in the Maltese archipelago. Nat. Hazards Earth Syst. Sci. 12, 1–21.
Gigli, G., Frodella, W., Garfagnoli, F., Morelli, S., Mugnai, F., Menna, F., Casagli, N., 2014. 3-D geomechanical rock mass characterization for the evaluation of rockslide susceptibility scenarios. Landslides 11, 131–140.
Hanssen, R.S., 2005. Satellite radar interferometry for deformationmonitoring: a priori assessment of feasibility and accuracy. Int. J. Appl. Earth Obs. Geoinf. 6, 253–260.
Herrera, G., Tómas, R., Monells, D., Centolanza, G., Mallorquí, J.J., Vicente, F., Navarro, V.D., Lopez-Sanchez, J.M., Sanabria, M., Cano, M., Mulas, J., 2010. Analysis of subsidence using TerraSAR-X data: Murcia case study. Eng. Geol. 116, 284–295.
Hooper, A., Zebker, H., Segall, P., Kampes, B., 2004. A new method for measuring deformation on volcanoes and other natural terrains using InSAR persistent scatterers. Geophys. Res. Lett. 31. http://dx.doi.org/10.1029/2004GL021737.
Hungr, O., Evans S., G., Bovis, M., Hutchinson, J.N., 2001. Review of the classification of landslides of the flow type. Environ. Eng. Geosci. 7, 221–238.
Hungr, O., Leroueil, S., Picarelli, L., 2014. The Varnes classification of landslide types, an update. Landslides 11, 167–194.
Hutchinson, J.N., 1988. General report: Morphological and geotechnical parameters of landslides in relation to geology and hydrology. In: Bonnard, C. (Ed.), Proceedings 5th International Symposium on Landslides, Lausanne, Switzerland. Balkema, Rotterdam, Netherlands, 1, pp. 3–35.
Intrieri, E., Gigli, G., Mugnai, F., Fanti, R., Casagli, N., 2012. Design and implementation of a landslide early warning system. Eng. Geol. 147-148 (12), 124–136.
Kasperski, J., Delacourt, C., Allemand, P., Potherat, P., Jaud, M., Varrel, E., 2010. Application of a terrestrial laser scanner (TLS) to the study of the Séchilienne landslide (Isère, France). Remote Sens. 2, 2785–2802.
Lambers, K., Eisenbeiss, H., Sauerbier, M., Kupferschmidt, D., Gaisecker, T., Sotoodeh, S., Hanusch, T., 2007. Combining photogrammetry and laser scanning for the recording and modeling of the late intermediate period site of Pinchango alto, Palpa, Peru. J. Archaeol. Sci. 34, 1702–1712.
Lim, M., Petley, D.N., Rosser, N.J., Allison, R.J., Long, A.J., Pybus, D., 2006. Combined digital photogrammetry and time-of-flight laser scanning for monitoring cliff evolution. Photogramm. Rec. 20 (1), 109–129.
Luzi, G., Pieraccini, M., Mecatti, D., Noferini, L., Guidi, G., Moia, F., Atzeni, C., 2004. Ground-based radar interferometry for landslides monitoring: atmospheric and instrumental decorrelation sources on experimental data. IEEE Trans. Geosci. Remote Sens. 42 (11), 2454–2466.
Massironi, M., Zampieri, D., Bianchi, M., Schiavo, A., Franceschini, A., 2009. Use of PSInSAR™ data to infer active tectonics: Clues on the differential uplift across the Giudicarie belt (central-eastern alps, Italy). Tectonophysics 476, 297–303.
Meisina, C., Zucca, F., Notti, D., Colombo, A., Cucchi, G., Giannico, C., Bianchi, M., 2008. Geological interpretation of PSInSAR data at regional scale. Sensors 8, 7469–7492.
Meisina, C., Notti, D., Zucca, F., Ceriani, M., Colombo, A., Poggi, F., Roccati, A., Zaccone, A., 2013. The use of PSInSAR™and SqueeSAR™techniques for updating landslide inventories. In: Margottini, C., Canuti, P., Sassa, K. (Eds.), Landslide Science and Practice. Springer, Berlin Heidelberg, pp. 81–87.
Nesci, O., Savelli, D., Diligenti, A., Marinangeli, D., 2005. Geomorphologicalsites in the northern marche (Italy). Examples from autochton anticline ridges and from val Marecchia allochton. Ital. J. Quat. Sci. 18, 79–91.
Noferini, L., Pieraccini, M., Mecatti, D., Macaluso, G., Atzeni, C., Mantovani, M., Marcato, G., Pasuto, A., Silvano, S., Tagliavini, F., 2007. Using GB-SAR technique to monitor slow moving landslide. Eng. Geol. 95, 88–98.
Nolesini, T., Di Traglia, F., Del Ventisette, C., Moretti, S., Casagli, N., 2013. Deformations and slope instability on Stromboli volcano: Integration of GBInSAR data and analog modeling. Geomorphology 180-181, 242–254.
Notti, D., Herrera, G., Bianchini, S., Meisina, C., García-Davalillo, J.C., Zucca, F., 2014. A methodology for improving landslide PSI data analysis. Int. J. Remote Sens. 35, 2186–2214.
Oppikofer, T., Jaboyedoff, M., Blikra, L., Derron, M.H., Metzer, R., 2009. Characterization and monitoring of the Åknes rockslide using terrestrial laser scanning. Nat. Hazards Earth Syst. Sci. 9, 1003–1019.
Panzera, E., D'Amico, S., Lotteri, A., Galea, P., Lombardo, G., 2012. Seismic site response of unstable steep slope using noise measurement: the case study of Xemxija Bay area. Malta. Nat. Hazards Earth Syst. Sci. 12, 3421–3431.
Paolucci, R., 2002. Amplification of earthquake ground motion by steep topographic irregularities. Earthq. Eng. Struct. Dyn. 31, 1831–1853.
Parker, A.L., Biggs, J., Lu, Z., 2014. Investigationg long-term subsidence at medicine Lake volcano, CA, using multitemporal InSAR. Geophys. J. Int. 199, 844–859.
Pasek, J., 1974. Gravitational block-type movements. Proc. Second Int. Congr. IAEG. Sao Paulo, Brasil, pp. V-PC-1.1–V-PC-1.9.
Pasuto, A., Soldati, M., 1996. Rock spreading. In: Dikau, R., Brunsden, D., Schrott, L., Ibsen, M.-L. (Eds.), Landslide Recognition: Identification, Movement and Causes. Wiley, Chichester, pp. 122–136.
Pasuto, A., Soldati, M., 2013. Lateral Spreading. In: Shroder, J.F. (Editor-in-chief), Marston, R.A., Stoffel, M. (Volume Editors). Treatise on Geomorphology, Vol 7, Mountain and Hillslope Geomorphology, San Diego: Academic Press. pp. 239–248.
Piacentini, D., Devoto, S., Mantovani, M., Alessandro Pasuto, A., Prampolini, M., Soldati, M., 2015. Landslide susceptibility modeling assisted by persistent scatterers interferometry (PSI): An example from the northwestern coast of Malta. Nat. Hazards 78, 681–697.
Pieraccini, M., Tarchi, D., Rudolf, H., Leva, D., Luzi, G., Bartoli, G., Atzeni, C., 2000. Structural static testing by interferometric synthetic radar. NDT and E Intl. 33, 565–570.
Pieraccini, M., Casagli, N., Luzi, G., Tarchi, D., Mecatti, D., Noferini, L., Atzeni, C., 2002. Landslide monitoring by ground-based radar interferometry: a field test in Valdarno (Italy). Int. J. Remote Sens. 24, 1385–1391.
Ponzana, L., 1993. Caratteri sedimentologici e petrografici della Formazione di Monte Morello (Eocene inferiore-medio, Appennino Settentrionale). Boll. Soc. Geol. Ital. 112, 201–218.
Pratesi, F., Nolesini, T., Bianchini, S., Leva, D., Lombardi, L., Fanti, R., Casagli, N., 2015. Early warning GBInSAR-based method for monitoring Volterra (Tuscany, Italy) City Walls. IEEE J. Selected Topics Appl. Earth Observ. Remote Sensing.
Raspini, F., Cigna, F., Moretti, S., 2012. Multi-temporal mapping of land subsidence at basin scale exploiting persistent scatterer interferometry: case study of Gioia Tauro plain (Italy). J. Maps 8, 514–524.
Raspini, F., Loupasakis, K., Rozos, D., Adam, N., Moretti, S., 2014. Ground subsidence phenomena in the Delta municipality region (Northern Greece): Geotechnical modeling and validation with persistent scatterer interferometry. Int. J. App. Earth Ob. Geo. Inf. 28, 78–89.
Raucoules, D., Colesanti, C., Carnec, C., 2007. Use of SAR interferometry for detecting and assessing ground subsidence. Compt. Rendus Geosci. 339, 289–302.
Ribacchi, R., Tommasi, P., 1988. Preservation and protection of the historical town of San Leo (Italy). IAEG Int. Symp. On Engineering Geology of Ancient Works, Monuments and Historical Sites, Athens. Vol. 1, pp. 55–64.
Riegl, 2010. Data sheet of Long Range & High Accuracy 3D terrestrial laser scanner LMSZ420i, [d_289_id-716.pdf] [Online]. (Available at) http://www.upc.edu/sct/documents_equipament/d_289_id-716.pdf.
Rosser, N.J., Petley, D.N., Lim, M., Dunning, S.A., Allison, R.J., 2005. Terrestrial laser scanning for monitoring the process of hard rock coastal cliff erosion. Q. J. Eng. Geol. Hydrogeol. 38, 363–375.
Rudolf, H., Leva, D., Tarchi, D., Sieber, A.J., 1999. A mobile and versatile SAR system. Proc. IGARSS 1, 592–594.
Slob, S., Hack, H.R.G.K., 2007. Fracture mapping using 3D laser scanning techniques. In: Sousa, L.R., Grossmann, C.O.N. (Eds.), 11th Congress of the International Society for Rock Mechanics: The Second Half Century of Rock Mechanics, 9–13, July 2007, Lisbon, Portugal, Vol. 1, pp. 299–302.
Slob, S., Hack, H.R.G.K., Turner, K., 2002. Approach to automate discontinuity measurements of rock faces using laser scanning techniques. In: Proceedings of ISRM EUROCK 2002: Funchal, Portugal, 25–28 November 2002/ed. by C. Dinid da Gama and L. Riberia e Sousa. Lisboa, Sociedade Portuguesa de Geotecnia. pp. 87-94.
Sousa, J.J., Ruiz, A.M., Hanssen, R.F., Bastos, L., Gil, A.J., Galindo-Zaldívar, J., Sanz de Galdeano, C., 2010. PS-InSAR processing methodologies in the detection of field surface deformation – Study of the Granada basin (central Betic cordilleras, Southern Spain). J. Geodyn. 49, 181–189.
Spreafico, M.C., Bacenetti, M., Borgatti, L., Perotti, L., Pellegrini, M., 2013. Structural analysis of San Leo (RN, Italy) east and north cliffs using 3D point clouds. Rend. Online Soc. Geol. Ital. 24, 304–306.
Tarchi, D., Ohlmer, E., Sieber, A.J., 1997. Monitoring of structural changes by radar interferometry. Res. Nondestruct. Eval. 9, 213–225.
Tarchi, D., Rudolf, H., Pieraccini, M., Atzeni, C., 2000. Remote monitoring of buildings using a ground-based SAR: application to cultural heritage survey. Int. J. Remote Sens. 21, 3545–3551.
Tarchi, D., Casagli, N., Fanti, R., Leva, D., Luzi, G., Pasuto, A., Pieraccini, M., Silvano, S., 2002. Landslide monitoring by using ground-based SAR interferometry: an example of application to the Tessina landslide in Italy. Eng. Geol. 68, 15–30.
Teza, G., Atzeni, C., Balzani, M., Galgaro, A., Galvani, G., Genevois, R., Luzi, G., Mecatti, D., Noferini, L., Pieraccini, M., Silvano, S., Uccelli, F., Zaltron, N., 2008. Ground-based monitoring of high risk landslide through joint use of laser scanning and interferometric radar. Int. J. Remote Sens. 29 (16), 4735–4756.
Tofani, V., Raspini, F., Catani, F., Casagli, N., 2013. Persistent scatterer interferometry (PSI) technique for landslide characterization and monitoring. Remote Sens. 5, 1045–1065.
Tommasi, P., Pellegrini, P., Boldini, D., Ribacchi, R., 2006. Influence of rainfall regime on hydraulic conditions and movement rates in the overconsolidated clayey slope of the Orvieto hill (Central Italy). Can. Geotech. J. 43, 70–86.
Trigila, A., Iadanza, C., Spizzichino, D., 2010. Quality assessment of the Italian landslide inventory using GIS processing. Landslides 7, 455–470.
Turner, A.K., Kemeny, J., Slob, S., Hack, H.R.G.K., 2006. Evaluation and management of unstable rock slopes by 3-D laser scanning. International association for engineering geology and the environment. Geol. Soc. Lond. 1–11.
Vilardo, G., Isaia, R., Ventura, G., De Martino, P., Terranova, C., 2010. InSAR permanent scatterer analysis reveals fault re-activation during inflation and deflation episodes at Campi Flegrei caldera. Remote Sens. Environ. 114, 2373–2383.
Vlcko, J., 2004. Extremely slow slope movements influencing the stability of Spis Castle, UNESCO site. Landslides 1, 67–71.
Vlcko, J., Greif, V., Grof, V., Jezny, M., Petro, L., Brcek, M., 2008. Rock displacement and thermal expansion study at historic heritage sites in Slovakia. Environ. Geol. 58, 1727–1740.
Yastikli, N., 2007. Documentation of cultural heritage using digital photogrammetry and laser scanning. J. Cult. Herit. 8, 423–427.
Zaruba, Q., Mencl, V., 1982. Landslides and their Control. second ed. Elsevier Scientific Pub. Co., Amsterdam (324 pp.).